

Nonequilibrium Peierls Transition

Shigeru AJISAKA^{*)}, Hisashi NISHIMURA
Shuichi TAsAKI and Ichiro TERAsAKI

*Advanced Institute for Complex Systems and Department of Applied Physics,
School of Science and Engineerings, Waseda University,
Tokyo 169-8555, Japan*

The nonequilibrium phase transition of an open Takayama-Lin Liu-Maki chain coupled with two reservoirs is investigated by combining a mean-field approximation and a formula characterizing nonequilibrium steady states, which is obtained from the algebraic field theoretical approach to nonequilibrium statistical mechanics. When the bias voltage is chosen as a control parameter, the phase transition between ordered and normal phases is found to be of first or second order. The current-voltage characteristics are S-shaped in some parameter region. In contrast, when the current is chosen as a control parameter, all the nontrivial solutions of the self-consistent equation are found to be stable. In this case, the phase transition between the ordered and normal phases is always of second order, and negative differential conductivity appears at low temperature.

§1. Introduction

One of the main interests in mesoscopic physics is a full understanding of the nonequilibrium properties of small quantum systems coupled with large reservoirs. When the reservoirs have different temperatures and/or chemical potentials, the whole system can be in a steady state with constant particle and energy flows, i.e. a nonequilibrium steady state (NESS). One of promising approaches in dealing with such systems is based on algebraic quantum field theory.^{1),2),3)} For example, with the aid of the algebraic approach, Pusz and Woronowicz rigorously derived Carnot's formula^{4),1)} and Ojima *et al.* proved the positivity of the (relative) entropy production rate,⁵⁾ both for systems of infinite degrees of freedom. In addition, for the XY model, a NESS was rigorously constructed.⁶⁾ Recently, starting from Ruelle's work on scattering-theoretical characterizations of NESS⁷⁾ and Jakšić-Pillet's investigation into entropy production,⁸⁾ the algebraic approach to NESS has been extensively developed [see Refs.9),10),11),12),13) and references therein]. Currently, linear response theories,¹⁴⁾ thermodynamic properties^{13),15)} and the Landauer-Büttiker formula^{16),17)} are investigated, in addition to various other aspects.¹⁸⁾

Hereafter, we consider a quantum system coupled with two free fermionic reservoirs L and R described by annihilation operators $a_{\mathbf{k}\sigma}$ and $b_{\mathbf{k}\sigma}$, respectively, where \mathbf{k} refers to the wave number and σ to the spin. In this case, if the reservoirs are initially set to be in different equilibria, the whole system is shown to approach a NESS in the long time limit provided that the *incoming* fields $\alpha_{\mathbf{k}\sigma}$ of $a_{\mathbf{k}\sigma}$ and $\beta_{\mathbf{k}\sigma}$ of $b_{\mathbf{k}\sigma}$ are complete.^{17),12)} The NESS so obtained can be characterized as a state satisfying Wick's theorem with respect to $\alpha_{\mathbf{k}\sigma}$ and $\beta_{\mathbf{k}\sigma}$ and having the two-point

^{*)} Email: g00k0056@suou.waseda.jp

functions:

$$\langle \alpha_{\mathbf{k}\sigma}^\dagger \alpha_{\mathbf{k}'\sigma'} \rangle_\infty = f_L(\hbar\omega_{kL})\delta_{\sigma\sigma'}\delta(\mathbf{k}-\mathbf{k}'), \quad \langle \beta_{\mathbf{k}\sigma}^\dagger \beta_{\mathbf{k}'\sigma'} \rangle_\infty = f_R(\hbar\omega_{kR})\delta_{\sigma\sigma'}\delta(\mathbf{k}-\mathbf{k}'), \quad (1\cdot 1)$$

where $\langle \dots \rangle_\infty$ stands for the average with respect to the NESS, $\hbar\omega_{k\nu}$ is the single-particle energy of wave number \mathbf{k} , $f_\nu(x) \equiv 1/(e^{(x-\mu_\nu)/T_\nu} + 1)$ is the Fermi distribution function, T_ν is the initial temperature and μ_ν is the initial chemical potential of the reservoir $\nu = L, R$. Formally, this can be understood as follows:^{*}) Let ρ_0 be an initial density matrix, where the two reservoirs are in distinct equilibria, and ρ_∞ be that of the NESS, then, $\lim_{t \rightarrow +\infty} e^{-iHt/\hbar}\rho_0 e^{iHt/\hbar} = \rho_\infty$ and, e.g., $\text{Tr}\{a_{\mathbf{k}\sigma}^\dagger a_{\mathbf{k}'\sigma'} \rho_0\} = f_L(\hbar\omega_{kL})\delta_{\sigma\sigma'}\delta(\mathbf{k}-\mathbf{k}')$. As the incoming field $\alpha_{\mathbf{k}\sigma}$ is given by $\lim_{t \rightarrow +\infty} e^{i\omega_{kL}(-t)} e^{iH(-t)/\hbar} a_{\mathbf{k}\sigma} e^{-iH(-t)/\hbar} = \alpha_{\mathbf{k}\sigma}$, one obtains the desired relation:

$$\begin{aligned} f_L(\hbar\omega_{kL})\delta_{\sigma\sigma'}\delta(\mathbf{k}-\mathbf{k}') &= \text{Tr}\{a_{\mathbf{k}\sigma}^\dagger a_{\mathbf{k}'\sigma'} \rho_0\} e^{i(\omega_{kL}-\omega_{k'L})t} \\ &= \text{Tr}\left\{ \left\{ e^{i\frac{H}{\hbar}(-t)} a_{\mathbf{k}\sigma} e^{-i\frac{H}{\hbar}(-t)} e^{i\omega_{kL}(-t)} \right\}^\dagger \left\{ e^{i\frac{H}{\hbar}(-t)} a_{\mathbf{k}'\sigma'} e^{-i\frac{H}{\hbar}(-t)} e^{i\omega_{k'L}(-t)} \right\} \rho_0 e^{i\frac{H}{\hbar}t} \right\} \\ &\rightarrow \text{Tr}\{ \alpha_{\mathbf{k}\sigma}^\dagger \alpha_{\mathbf{k}'\sigma'} \rho_\infty \} \equiv \langle \alpha_{\mathbf{k}\sigma}^\dagger \alpha_{\mathbf{k}'\sigma'} \rangle_\infty \quad (\text{as } t \rightarrow +\infty). \end{aligned} \quad (1\cdot 2)$$

As noted by Blanter and Büttiker¹⁹⁾ [cf. Eqs.(29) and (36) in their paper], the NESS characterization (1·1) can be a starting point for the Landauer-Büttiker approach to transport properties of mesoscopic circuits. Note also that (1·1) can be applied even to systems with interacting fermions if the incoming fields are complete.¹²⁾ Indeed, Katsura successfully derived a NESS from (1·1) for a solvable model of the Kondo effect.²⁰⁾

Since eq.(1·1) fully characterizes NESSes of noninteracting fermions, it is natural to consider a mean-field approximation based on (1·1) for a NESS of interacting fermions. Based on this view, we investigated a NESS of an Aharonov-Bohm ring with a quantum dot within a mean-field approximation and obtained a differential conductivity consistent with numerical renormalization group analysis and experiments.²¹⁾ Here, with the aid of a similar nonequilibrium mean-field approximation, we study the nonequilibrium phase transition in the Takayama-Lin Liu-Maki chain²²⁾ (TLM chain) embedded between two infinitely extended reservoirs. The TLM chain is a continuum limit of a lattice model (the SSH lattice) for polyacetylene proposed by Su, Schrieffer and Heeger²³⁾ and describes the charge density wave commensurate with the lattice.

We employ the TLM chain as a representative example of systems with phase transitions. However, since the mean field approximations of the TLM chain, a superconductors, a 1D extended Hubbard lattice of spinless fermions and the Jordan-Wigner-transformed XXZ model are equivalent, the present analysis would provide some insight into nonequilibrium properties of various interacting systems, such as the current-induced suppression of the charge order observed in some θ -type BEDT-TTF organic conductors^{24),25),26),27)} and the negative differential conductivity recently reported for the XXZ model²⁸⁾ and some strongly correlated systems.^{29),30),31)}

The rest of this paper is arranged as follows. In Sec. 2, we introduce a finite TLM chain coupled with two infinitely extended reservoirs. In Sec. 3, a mean-field

^{*}) The very proof of the existence of the limits requires rigorous and careful arguments.¹²⁾

approximation based on (1.1) is discussed. The averaged lattice distortion serves as an order parameter, and its self-consistent equation is obtained by averaging the equation of motion of the lattice distortion with respect to a nonequilibrium steady state. In Sec. 4, the self-consistent equation, current and stability conditions are explicitly derived in case where the TLM chain is long enough and the order parameter is spatially uniform. In Sec. 5, possible phases are discussed in detail when the chain-reservoir couplings are symmetric. When the bias voltage is chosen as one of the control parameters, the phase transition between ordered and normal phases could be of first or second order depending on the bias voltage and temperature. At low temperature, the current-voltage characteristics are S-shaped. For some bias-voltages, the temperature dependence of the order parameter is found to be similar to that for the nonequilibrium superconducting phase induced by excess quasiparticles.^{32),33)} In contrast, when the current is chosen as one of the control parameters, the self-consistent equation has a unique stable solution and the phase transition between the ordered and normal phases is always of second order. Negative differential conductivity appears when the temperature is lower than a certain threshold value. In Sec. 6, after a summary of the paper is given, the self-consistent equation for the open TLM chain is compared with that for the nonequilibrium superconductor obtained by Scalapino *et al.*³²⁾ Then, on the basis of the similarity of mean-field approximations of the open TLM chain and an open 1D extended Hubbard lattice, the experimental results for some θ -type BEDT-TTF organic conductors^{24), 25), 26), 27)} as well as the negative differential conductivity found in an open XXZ model²⁸⁾ are qualitatively discussed within the scope of the present analysis. In Appendix A, an open TLM chain is derived from an open SSH lattice. In Appendix B, normal-mode operators are explicitly given. In Appendix C, we discuss the relationship between the average chemical potential and the Coulomb energy. In Appendix D, Green functions necessary for deriving the self-consistent equation are provided. In Appendix E, the stability of the nontrivial phases at zero temperature is discussed. In Appendix F, the Ginzburg-Landau expansion for the self-consistent equation is given.

§2. Open TLM Model

The system in question consists of a finite TLM chain and two free electron reservoirs. In terms of the quantized local lattice distortion $\Delta(x)$ and the two-component electron field $\Psi_\sigma(x)$

$$\Psi_\sigma(x) \equiv \begin{pmatrix} d_\sigma(x) \\ e_\sigma(x) \end{pmatrix}, \quad (2.1)$$

the Hamiltonian of the TLM chain is given by²²⁾

$$\begin{aligned} H_S = & \sum_\sigma \int_0^\ell dx \Psi_\sigma^\dagger(x) \left[-i\hbar v \sigma_y \frac{\partial}{\partial x} + \Delta(x) \sigma_x \right] \Psi_\sigma(x) \\ & + \frac{1}{2\pi\hbar v \lambda} \int_0^\ell dx \left[\Delta(x)^2 + \frac{1}{\omega_0^2} \Pi(x)^2 \right], \end{aligned} \quad (2.2)$$

where ℓ is the length of the system, v is the Fermi velocity, σ_x and σ_y are the x and y components of Pauli matrices, λ is the dimensionless coupling constant, ω_0 is the phonon frequency and $\Pi(x)$ corresponds to the momentum conjugate to $\Delta(x)$. Nonvanishing equal-time commutation relations among those operators are

$$\{d_\sigma(x), d_{\sigma'}(y)^\dagger\} = \{e_\sigma(x), e_{\sigma'}(y)^\dagger\} = \delta_{\sigma,\sigma'}\delta(x-y), \quad (2.3)$$

$$[\Delta(x), \Pi(y)] = i\hbar^2\pi\lambda v\omega_0^2\delta(x-y), \quad (2.4)$$

where $\{A, B\} = AB + BA$ and $[A, B] = AB - BA$. As the system is finite, electron waves are reflected back at the edges, and the following boundary condition is imposed:

$$d_\sigma(0) = 0, \quad e_\sigma(\ell) = 0. \quad (2.5)$$

The fields d_σ and e_σ correspond to electrons at even and odd sites, respectively, of a finite SSH lattice (cf. Appendix A). Note that, instead of d_σ and e_σ , the original work²²⁾ uses the right- and left-moving electron fields $\psi_{R\sigma}(x)$ and $\psi_{L\sigma}(x)$, respectively,

$$\psi_{R\sigma}(x) = \frac{1}{\sqrt{2}}\{d_\sigma(x) - ie_\sigma(x)\}, \quad \psi_{L\sigma}(x) = \frac{1}{\sqrt{2}}\{e_\sigma(x) - id_\sigma(x)\}. \quad (2.6)$$

The reservoirs are described by

$$H_B = \sum_\sigma \int d\mathbf{k} \{ \hbar\omega_{kL} a_{\mathbf{k}\sigma}^\dagger a_{\mathbf{k}\sigma} + \hbar\omega_{kR} b_{\mathbf{k}\sigma}^\dagger b_{\mathbf{k}\sigma} \}, \quad (2.7)$$

where $a_{\mathbf{k}\sigma}$ and $b_{\mathbf{k}\sigma}$ stand for the annihilation operators of electrons with wave number \mathbf{k} and spin σ in the left and right reservoirs, respectively, and $\hbar\omega_{k\nu}$ ($\nu = L, R$) are their energies measured from the zero-bias chemical potentials at absolute zero temperature. The nonvanishing anticommutation relations among them are $\{a_{\mathbf{k}\sigma}, a_{\mathbf{k}'\sigma'}^\dagger\} = \{b_{\mathbf{k}\sigma}, b_{\mathbf{k}'\sigma'}^\dagger\} = \delta_{\sigma\sigma'}\delta(\mathbf{k} - \mathbf{k}')$. The chain-reservoir interaction is assumed to be

$$V = \sum_\sigma \int d\mathbf{k} \left\{ \hbar v_{\mathbf{k}} e_{\sigma}^\dagger(0) a_{\mathbf{k}\sigma} + \hbar w_{\mathbf{k}} d_{\sigma}^\dagger(\ell) b_{\mathbf{k}\sigma} + (h.c.) \right\}, \quad (2.8)$$

where $v_{\mathbf{k}}$ and $w_{\mathbf{k}}$ stand for the coupling matrix elements.

The Hamiltonian of the whole system is given by

$$H = H_S + V + H_B. \quad (2.9)$$

As will be discussed in Appendix A, an open TLM chain described by H corresponds to an open SSH lattice that couples with the reservoirs through the end sites and the number of whose sites is a multiple of four.

From (2.9), the lattice distortion Δ is found to obey the following equation of motion:

$$\begin{aligned} \frac{\partial \Delta(x, t)}{\partial t} &= \frac{1}{i\hbar} [\Delta(x, t), H] = \Pi(x, t) \\ \frac{\partial^2 \Delta(x, t)}{\partial t^2} &= \frac{\partial \Pi(x, t)}{\partial t} = -\omega_0^2 \left(\Delta(x, t) + \pi\hbar v\lambda \sum_\sigma \Psi_\sigma^\dagger(x, t) \sigma_x \Psi_\sigma(x, t) \right). \end{aligned} \quad (2.10)$$

Eqs.(2.9) and (2.10) are our starting points.

§3. NESS Mean-Field Approximation

In this section, we describe a procedure for evaluating the NESS averages of the electron variables for the TLM chain and derive the self-consistent equation for the NESS average $\overline{\Delta}(x) \equiv \langle \Delta(x) \rangle_\infty$ of the lattice distortion, which serves as the order parameter of the Peierls transition.

The nonequilibrium steady state under the mean-field approximation is characterized by (1.1) where $\alpha_{\mathbf{k}\sigma}$ and $\beta_{\mathbf{k}\sigma}$ are the incoming fields of $a_{\mathbf{k}\sigma}$ and $b_{\mathbf{k}\sigma}$ with respect to the mean-field Hamiltonian:

$$H_{\text{MF}} = H_S^{\text{MF}} + V + H_B \quad (3.1)$$

$$H_S^{\text{MF}} \equiv \sum_\sigma \int_0^\ell dx \Psi_\sigma^\dagger(x) \left[-i\hbar v \sigma_y \frac{\partial}{\partial x} + \overline{\Delta}(x) \sigma_x \right] \Psi_\sigma(x). \quad (3.2)$$

Namely, they are defined as the solution of

$$\frac{1}{\hbar} [\alpha_{\mathbf{k}\sigma}, H_{\text{MF}}] = \omega_{kL} \alpha_{\mathbf{k}\sigma}, \quad e^{iH_{\text{MF}}t/\hbar} \alpha_{\mathbf{k}\sigma} e^{-iH_{\text{MF}}t/\hbar} e^{i\omega_{kL}t} \rightarrow \alpha_{\mathbf{k}\sigma} \quad (t \rightarrow -\infty) \quad (3.3)$$

$$\frac{1}{\hbar} [\beta_{\mathbf{k}\sigma}, H_{\text{MF}}] = \omega_{kR} \beta_{\mathbf{k}\sigma}, \quad e^{iH_{\text{MF}}t/\hbar} \beta_{\mathbf{k}\sigma} e^{-iH_{\text{MF}}t/\hbar} e^{i\omega_{kR}t} \rightarrow \beta_{\mathbf{k}\sigma} \quad (t \rightarrow -\infty) \quad (3.4)$$

Since the mean-field Hamiltonian H_{MF} is bilinear with respect to the electron creation/annihilation operators, the incoming fields are linear combinations of $a_{\mathbf{k}\sigma}$, $b_{\mathbf{k}\sigma}$, and $\Psi_\sigma(x)$. As shown in Appendix B, the incoming fields are fully determined by (3.3) and (3.4). Conversely, the original operators can be represented by the incoming fields. For example, we have

$$\Psi_\sigma(x) = \int d\mathbf{k} \left\{ v_{\mathbf{k}} \frac{h(x; \omega_{kL})}{\Lambda_-(\omega_{kL})^*} \alpha_{\mathbf{k}\sigma} + w_{\mathbf{k}} \frac{\tilde{h}(x; \omega_{kR})}{\Lambda_-(\omega_{kR})^*} \beta_{\mathbf{k}\sigma} \right\}, \quad (3.5)$$

where $\Lambda_-(\omega)$, $h(x; \omega)$ and $\tilde{h}(x; \omega)$ are auxiliary functions given by

$$\begin{aligned} \Lambda_-(\omega) &= 1 - \xi_-(\omega) g_{--}(0, 0; \omega) - \eta_-(\omega) g_{++}(\ell, \ell; \omega) \\ &\quad + \xi_-(\omega) \eta_-(\omega) \{ g_{++}(\ell, \ell; \omega) g_{--}(0, 0; \omega) - g_{+-}(\ell, 0; \omega) g_{-+}(0, \ell; \omega) \}, \end{aligned} \quad (3.6)$$

$$\begin{aligned} h(x; \omega) &= G(x, 0; \omega) \begin{pmatrix} 0 \\ 1 \end{pmatrix} \{ 1 - g_{++}(\ell, \ell; \omega) \eta_+(\omega) \} \\ &\quad + G(x, \ell; \omega) \begin{pmatrix} 1 \\ 0 \end{pmatrix} g_{+-}(\ell, 0; \omega) \eta_+(\omega), \end{aligned} \quad (3.7)$$

$$\begin{aligned} \tilde{h}(x; \omega) &= G(x, 0; \omega) \begin{pmatrix} 0 \\ 1 \end{pmatrix} g_{-+}(0, \ell; \omega) \xi_+(\omega) \\ &\quad + G(x, \ell; \omega) \begin{pmatrix} 1 \\ 0 \end{pmatrix} \{ 1 - g_{--}(0, 0; \omega) \xi_+(\omega) \}, \end{aligned} \quad (3.8)$$

$$\xi_\pm(\omega) = \int d\mathbf{k}' \frac{|v_{\mathbf{k}'}|^2}{\omega - \omega_{k'L} \pm i0}, \quad \eta_\pm(\omega) = \int d\mathbf{k}' \frac{|w_{\mathbf{k}'}|^2}{\omega - \omega_{k'R} \pm i0}. \quad (3.9)$$

And the Green function G for the finite TLM chain and, equivalently, its components $g_{\sigma\sigma'}$ ($\sigma, \sigma' = \pm$) are defined as a solution of

$$G(x, y; \omega) \equiv \begin{pmatrix} g_{++}(x, y; \omega) & g_{+-}(x, y; \omega) \\ g_{-+}(x, y; \omega) & g_{--}(x, y; \omega) \end{pmatrix}, \quad (3.10)$$

$$\left[-i\hbar v \sigma_y \frac{\partial}{\partial x} + \overline{\Delta}(x) \sigma_x \right] G(x, y; \omega) = \hbar\omega G(x, y; \omega) - \hbar \mathbf{1} \delta(x - y), \quad (3.11)$$

$$g_{++}(0, y; \omega) = g_{+-}(0, y; \omega) = g_{-+}(\ell, y; \omega) = g_{--}(\ell, y; \omega) = 0. \quad (3.12)$$

For the derivation of incoming-field operators, see Appendix B. Then, the mean-field NESS is given as a state satisfying Wick's theorem with respect to $\alpha_{\mathbf{k}\sigma}$ and $\beta_{\mathbf{k}\sigma}$ with the two-point functions (1.1). Note that, although the Green function (and, thus, Λ_-, h and \tilde{h}) diverges as a function of ω at eigenvalues of the differential operator in the left-hand side of (3.11), the integrand of (3.5) remains finite even when ω_{kL} or ω_{kR} is equal to one of the eigenvalues. The NESS average of any electron variable consisting of Ψ_σ can be calculated from (1.1) and (3.5).

The self-consistent equation for the order parameter $\overline{\Delta}(x)$ is derived from the equation of motion (2.10) for the lattice distortion. Because of the time-independence of $\overline{\Delta}(x)$, (2.10) leads to

$$0 = \frac{-1}{\omega_0^2} \frac{\partial^2 \overline{\Delta}(x)}{\partial t^2} = \overline{\Delta}(x) + \pi \hbar v \lambda \sum_{\sigma} \langle \Psi_{\sigma}^{\dagger}(x) \sigma_x \Psi_{\sigma}(x) \rangle_{\infty}. \quad (3.13)$$

Using (1.1) and (3.5), $\int d\mathbf{k} |v_{\mathbf{k}}|^2 F(\omega_{kL}) = \int_{-\infty}^{\infty} d\omega F(\omega) \text{Im} \xi_{-}(\omega) / \pi$ and a similar formula for $\eta_{-}(\omega)$, the self-consistent equation (3.13) reads as

$$\frac{2}{\pi} \int_{-\infty}^{\infty} d\omega \left\{ \text{Im} \xi_{-}(\omega) \frac{h(x; \omega)^{\dagger} \sigma_x h(x; \omega)}{|\Lambda_{-}(\omega)|^2} f_L(\hbar\omega) + \text{Im} \eta_{-}(\omega) \frac{\tilde{h}(x; \omega)^{\dagger} \sigma_x \tilde{h}(x; \omega)}{|\Lambda_{-}(\omega)|^2} f_R(\hbar\omega) \right\} = -\frac{\overline{\Delta}(x)}{\pi \hbar v \lambda}, \quad (3.14)$$

where we use the convention $\text{Im} \xi_{-}(\omega) = 0$ ($\text{Im} \eta_{-}(\omega) = 0$) for ω outside the range of ω_{kL} (ω_{kR}). Equation (3.14) is the self-consistent equation for the order parameter $\overline{\Delta}(x)$.

§4. Spatially Uniform Phase

4.1. Self-consistent equation

Hereafter, we consider the cases where the chain is half-filled; namely, the zero-bias chemical potentials are located at the band centre of the TLM chain. Then, in order to prevent an increase in electrostatic energy, the chemical potentials of the reservoirs should be chosen such that $\mu_L = -\mu_R = -eV/2$ where V is the bias voltage and e is the elementary charge (for details, see Appendix C). It is well known²²⁾

that the energy cutoff $\hbar\omega_c$ ($\hbar\omega_c \gg T, e|V|$) is necessary for the TLM model, and the integration interval of (3.14) should be replaced with $(-\omega_c, \omega_c)$.

The local state of the TLM chain within a certain region of the boundary is affected by the existence of the reservoirs. However, if the chain-reservoir interaction is not too strong and if the size of this region is much smaller than the length of the chain, boundary effects might be neglected. From this observation, we study the uniform phase where the order parameter is independent of the coordinate: $\overline{\Delta}(x) = \overline{\Delta}$. In this subsection, we derive the self-consistent equation for $\overline{\Delta}$ when the TLM chain is sufficiently long.

When the order parameter is spatially uniform, the Green function defined by (3.11) can be easily obtained for any real number ω and we have (for its complete expression, see Appendix D)

$$g_{++}(x, \ell; \omega) = g_{--}(\ell - x, 0; \omega) = -\frac{\hbar\omega \sin \kappa x}{vD(\omega)}, \quad (4.1)$$

$$g_{-+}(x, \ell; \omega) = g_{+-}(\ell - x, 0; \omega) = -\frac{\hbar\kappa v \cos \kappa x + \overline{\Delta} \sin \kappa x}{vD(\omega)}, \quad (4.2)$$

where $\kappa = \sqrt{(\hbar\omega)^2 - \overline{\Delta}^2}/(\hbar v)$ and $D(\omega) = \hbar\kappa v \cos \kappa \ell + \overline{\Delta} \sin \kappa \ell$. Then, the second term of the left-hand side of (3.14) reads as

$$\begin{aligned} & \int_{|\omega| < \omega_c} d\omega \text{Im}\eta_-(\omega) \frac{\tilde{h}(x; \omega)^\dagger \sigma_x \tilde{h}(x; \omega)}{|\Lambda_-(\omega)|^2} f_R(\hbar\omega) \\ &= \int_{|\omega| < \omega_c} d\omega \frac{\text{Im}\eta_-(\omega) f_R(\hbar\omega)}{|v^2 D(\omega) \Lambda_-(\omega)|^2} \left\{ \hbar^2 \kappa v \omega (v^2 - |\xi_-(\omega)|^2) \sin 2\kappa x \right. \\ & \quad \left. - (\hbar\omega v^2 \overline{\Delta} + 2v(\hbar\omega)^2 \text{Re}\xi_-(\omega) + \hbar\omega \overline{\Delta} |\xi_-(\omega)|^2) \cos 2\kappa x \right. \\ & \quad \left. + \hbar v^2 \overline{\Delta} \left(\omega + \frac{2\overline{\Delta}}{\hbar v} \text{Re}\xi_-(\omega) + \frac{\omega}{v^2} |\xi_-(\omega)|^2 \right) \right\} \text{sgn}(|\hbar\omega| - |\overline{\Delta}|), \quad (4.3) \end{aligned}$$

where the denominator is a function of ω and $\kappa\ell$: $|v^2 D(\omega) \Lambda_-(\omega)|^2 \equiv |\tilde{\Lambda}_-(\omega, \kappa\ell)|^2$ with

$$\begin{aligned} \tilde{\Lambda}_-(\omega, \theta) &= \hbar\kappa v (v^2 - \xi_-(\omega) \eta_-(\omega)) \cos \theta \\ & \quad + (v^2 \overline{\Delta} + v\hbar\omega \{\xi_-(\omega) + \eta_-(\omega)\} + \overline{\Delta} \xi_-(\omega) \eta_-(\omega)) \sin \theta. \quad (4.4) \end{aligned}$$

Now we show that (4.3) is simplified when the TLM chain is sufficiently long. It is easy to see that if $|\hbar\omega| < |\overline{\Delta}|$, κ is purely imaginary, $|D(\omega)|^2 \tilde{h}(x; \omega)^\dagger \sigma_x \tilde{h}(x; \omega) \sim e^{2|\kappa|x}$ and $|D(\omega) \Lambda_-(\omega)|^2 \sim e^{2|\kappa|\ell}$. Then, the integrand of (4.3) is on the order of

$$\frac{\tilde{h}(x; \omega)^\dagger \sigma_x \tilde{h}(x; \omega)}{|\Lambda_-(\omega)|^2} \sim e^{-2|\kappa|(\ell-x)}, \quad (4.5)$$

which is negligible for large ℓ unless x is near the chain ends. Hence, the contribution to (4.3) from the interval $0 < \omega < |\overline{\Delta}|/\hbar$ is negligible. This implies that $|\overline{\Delta}|$ corresponds to the electronic energy gap as in the equilibrium case.

On the other hand, if $|\hbar\omega| > |\bar{\Delta}|$, κ is real. Then, with the aid of the Fourier expansion of $1/|\tilde{\Lambda}_-(\omega, \theta)|^2$,

$$\frac{1}{|\tilde{\Lambda}_-(\omega, \theta)|^2} = \sum_{n=-\infty}^{\infty} \frac{e^{2ni\theta}}{\zeta_n(\omega)},$$

where $1/\zeta_n(\omega)$ is the Fourier coefficient, one can show that the first and second terms of the right-hand side of (4.3) are negligible, and that the denominator in the third term is replaced with $\zeta_0(\omega)$ provided ℓ is large and x is far from the chain ends. For example, the first term of (4.3) becomes

$$\begin{aligned} & \int_{|\bar{\Delta}|/\hbar < |\omega| < \omega_c} d\omega \frac{\text{Im}\eta_-(\omega) f_R(\hbar\omega)}{|v^2 D(\omega) \Lambda_-(\omega)|^2} \hbar^2 \kappa v \omega (v^2 - |\xi_-(\omega)|^2) \sin 2\kappa x \\ &= \sum_{n=-\infty}^{\infty} \int_{|\bar{\Delta}|/\hbar < |\omega| < \omega_c} \frac{d\omega H(\omega)}{2i \zeta_n(\omega)} \{e^{2i\kappa(n\ell+x)} - e^{2i\kappa(n\ell-x)}\}, \end{aligned} \quad (4.6)$$

where $H(\omega) = \text{Im}\eta_-(\omega) f_R(\hbar\omega) \hbar^2 \kappa v \omega (v^2 - |\xi_-(\omega)|^2)$. When x is far from the chain ends, $n\ell \pm x = O(\ell)$ and (4.6) is negligible for large ℓ thanks to the Riemann-Lebesgue lemma. In short, (4.3) is found to be

$$\begin{aligned} & \int_{|\omega| < \omega_c} d\omega \text{Im}\eta_-(\omega) \frac{\tilde{h}(x; \omega)^\dagger \sigma_x \tilde{h}(x; \omega)}{|\Lambda_-(\omega)|^2} f_R(\hbar\omega) \\ &= \hbar v^2 \bar{\Delta} \int_{\frac{|\bar{\Delta}|}{\hbar} < |\omega| < \omega_c} d\omega \frac{\text{Im}\eta_-(\omega)}{\zeta_0(\omega)} f_R(\hbar\omega) \left(\omega + \frac{2\bar{\Delta}}{\hbar v} \text{Re}\xi_-(\omega) + \frac{\omega}{v^2} |\xi_-(\omega)|^2 \right). \end{aligned} \quad (4.7)$$

By a similar argument, when the TLM chain is sufficiently long, the self-consistent equation (3.14) gives the desired equation for $\bar{\Delta}$

$$\bar{\Delta} = 0 \quad \text{or} \quad (4.8)$$

$$\frac{-1}{\lambda} = S(\bar{\Delta}, V, T_L, T_R), \quad (4.9)$$

where

$$\begin{aligned} \frac{S(\bar{\Delta}, V, T_L, T_R)}{2\hbar^2 v^3} &\equiv \int_{\frac{|\bar{\Delta}|}{\hbar} < |\omega| < \omega_c} d\omega \left\{ \frac{\text{Im}\xi_-(\omega)}{\zeta_0(\omega)} \left(\omega + \frac{2\bar{\Delta}}{\hbar v} \text{Re}\eta_-(\omega) + \frac{\omega}{v^2} |\eta_-(\omega)|^2 \right) f_L(\hbar\omega) \right. \\ &\quad \left. + \frac{\text{Im}\eta_-(\omega)}{\zeta_0(\omega)} \left(\omega + \frac{2\bar{\Delta}}{\hbar v} \text{Re}\xi_-(\omega) + \frac{\omega}{v^2} |\xi_-(\omega)|^2 \right) f_R(\hbar\omega) \right\}. \end{aligned} \quad (4.10)$$

The function $\zeta_0(\omega)$ in the denominators is easily calculated as

$$\zeta_0(\omega) = \hbar^2 v^4 \kappa \left| \text{Im}\xi_-(\omega) \left\{ \omega + \frac{2\bar{\Delta}}{\hbar v} \text{Re}\eta_-(\omega) + \frac{\omega}{v^2} |\eta_-(\omega)|^2 \right\} \right. \quad (4.11)$$

$$\left. + \text{Im}\eta_-(\omega) \left\{ \omega + \frac{2\bar{\Delta}}{\hbar v} \text{Re}\xi_-(\omega) + \frac{\omega}{v^2} |\xi_-(\omega)|^2 \right\} \right|. \quad (4.12)$$

4.2. Electric current

As easily seen, the electric current at x in the TLM chain is given by

$$J(x) = -ev \sum_{\sigma} \Psi_{\sigma}^{\dagger}(x) \sigma_y \Psi_{\sigma}(x) , \quad (4.13)$$

and its NESS average by

$$\bar{J} = \langle J(x) \rangle_{\infty} = -\frac{4ev^2}{\pi} \int_{-\omega_c}^{\omega_c} d\omega (\hbar\kappa v)^2 \frac{\text{Im}\eta_{-}(\omega)\text{Im}\xi_{-}(\omega)}{|v^2 D(\omega)\Lambda_{-}(\omega)|^2} \left(f_L(\hbar\omega) - f_R(\hbar\omega) \right) .$$

As in the case of the self-consistent equation, for large ℓ , the averaged current reduces to

$$\bar{J} = -\frac{4ev^2}{\pi} \int_{\frac{|\bar{\Delta}|}{\hbar} < |\omega| < \omega_c} d\omega (\hbar\kappa v)^2 \frac{\text{Im}\eta_{-}(\omega)\text{Im}\xi_{-}(\omega)}{\zeta_0(\omega)} \left(f_L(\hbar\omega) - f_R(\hbar\omega) \right) . \quad (4.14)$$

4.3. Stability

Since no general thermodynamic criterion is available for discussing the stabilities of NESS, we study the phase stability based on the linear stability of the adiabatic evolution equation for a spatially uniform order parameter.

Within the adiabatic approximation, the force on the order parameter from the electrons is given by $\pi\hbar v\lambda \sum_{\sigma} \langle \Psi_{\sigma}^{\dagger}(x) \sigma_x \Psi_{\sigma}(x) \rangle_{\infty}$, where the order parameter is replaced with its instantaneous value $\tilde{\Delta}(t)$. Then, we have

$$\frac{\partial^2 \tilde{\Delta}(t)}{\partial t^2} = -\omega_0^2 \left\{ 1 + \lambda S(\tilde{\Delta}(t), V, T_L, T_R) \right\} \tilde{\Delta}(t) , \quad (4.15)$$

where the function $S(\tilde{\Delta}, V, T_L, T_R)$ is defined by (4.10).

First, we consider the stability of the normal phase where $\bar{\Delta} = 0$. As the linearized equation for $\tilde{\Delta}(t)$ is given by

$$\frac{\partial^2 \tilde{\Delta}(t)}{\partial t^2} = -\omega_0^2 \left\{ 1 + \lambda S(0, V, T_L, T_R) \right\} \tilde{\Delta}(t) ,$$

the phase is stable when

$$\chi_N \equiv 1 + \lambda S(0, V, T_L, T_R) > 0 . \quad (4.16)$$

Next, we investigate the stability of the phase with nonvanishing $\bar{\Delta}$. Then, two cases should be distinguished: the constant-bias-voltage and constant-current cases. In the former, the linearized equation for $\delta\tilde{\Delta}(t) = \tilde{\Delta}(t) - \bar{\Delta}$ is

$$\frac{\partial^2 \tilde{\Delta}(t)}{\partial t^2} = -\omega_0^2 \lambda \bar{\Delta} \left(\frac{\partial S}{\partial \bar{\Delta}} \right)_V \delta\tilde{\Delta}(t) ,$$

and the phase is stable when

$$\chi_V(\bar{\Delta}) = \lambda \bar{\Delta} \left(\frac{\partial S}{\partial \bar{\Delta}} \right)_V > 0 . \quad (4.17)$$

In the latter case, the linearized equation is

$$\frac{\partial^2 \tilde{\Delta}(t)}{\partial t^2} = -\omega_0^2 \lambda \bar{\Delta} \left(\frac{\partial S}{\partial \bar{\Delta}} \right)_{\bar{J}} \delta \tilde{\Delta}(t),$$

and the phase is stable when

$$\begin{aligned} \chi_I(\bar{\Delta}) &= \lambda \bar{\Delta} \left(\frac{\partial S}{\partial \bar{\Delta}} \right)_{\bar{J}} \\ &= \lambda \bar{\Delta} \left\{ \left(\frac{\partial S}{\partial \bar{\Delta}} \right)_V - \left(\frac{\partial S}{\partial V} \right)_{\bar{\Delta}} \left(\frac{\partial \bar{J}}{\partial \bar{\Delta}} \right)_V / \left(\frac{\partial \bar{J}}{\partial V} \right)_{\bar{\Delta}} \right\} > 0. \end{aligned} \quad (4.18)$$

As will be shown in Appendix E, the phase with a nontrivial order parameter at constant current is more stable than that at constant bias voltage.

§5. Nonequilibrium Phase Transitions

5.1. Basic formula

In this section, we study the nonequilibrium phase transitions when the TLM chain couples symmetrically with two identical reservoirs at temperature T : $|v_{\mathbf{k}}| = |w_{\mathbf{k}}|$, $\omega_{kL} = \omega_{kR}$, and $T_L = T_R = T$. Since $\eta_-(\omega) = \xi_-(\omega)$ and

$$\frac{\omega + \frac{2\bar{\Delta}}{\hbar v} \text{Re}\eta_-(\omega) + \frac{\omega}{v^2} |\eta_-(\omega)|^2}{\left| \omega + \frac{2\bar{\Delta}}{\hbar v} \text{Re}\eta_-(\omega) + \frac{\omega}{v^2} |\eta_-(\omega)|^2 \right|} = \text{sgn}(\omega)$$

for $|\hbar\omega| > |\bar{\Delta}|$ where $\text{sgn}(\omega)$ the sign of ω , we have

$$S(\bar{\Delta}, V, T_L, T_R) \Big|_{T_L=T_R=T} \equiv S(\bar{\Delta}, V, T) = \int_{\frac{|\bar{\Delta}|}{\hbar} < |\omega| < \omega_c} \frac{d\omega}{\kappa v} \text{sgn}(\omega) \{f_L(\hbar\omega) + f_R(\hbar\omega)\}.$$

Thus, the self-consistent equation (4.9) becomes

$$\frac{1}{\lambda} = -S(\bar{\Delta}, V, T) = \int_{|\bar{\Delta}|}^{\hbar\omega_c} \frac{d\epsilon}{\sqrt{\epsilon^2 - \bar{\Delta}^2}} \frac{2 \sinh(\epsilon/T)}{\cosh(\frac{eV}{2T}) + \cosh(\epsilon/T)}. \quad (5.1)$$

Since the current is carried by electrons having energies near the Fermi energies, we further approximate $\xi_-(\omega) = \eta_-(\omega) = iw_0$ and we have

$$\begin{aligned} \bar{J} &= -\frac{2evw_0}{\pi(v^2 + w_0^2)} \int_{\frac{|\bar{\Delta}|}{\hbar} < |\omega| < \omega_c} d\omega \frac{\kappa v}{|\omega|} (f_L(\hbar\omega) - f_R(\hbar\omega)) \\ &= \frac{2G_0}{e} \int_{|\bar{\Delta}|}^{\hbar\omega_c} d\epsilon \frac{\sqrt{\epsilon^2 - \bar{\Delta}^2}}{\epsilon} \frac{\sinh(\frac{eV}{2T})}{\cosh(\frac{eV}{2T}) + \cosh(\frac{\epsilon}{T})}, \end{aligned} \quad (5.2)$$

where the normal-state conductance G_0 is given by

$$G_0 = \frac{e^2}{\pi\hbar} \frac{2vw_0}{v^2 + w_0^2} . \quad (5.3)$$

Indeed, if $\bar{\Delta} = 0$ and terms on the order of $\exp\{-(2\hbar\omega_c - e|V|)/(2T)\}$ are neglected, one can easily evaluate the integral in (5.2), yielding

$$\bar{J} = G_0 V ,$$

irrespective of the temperature T . In the rest of this section, the phase transition and nonlinear conduction will be discussed based on (5.1) and (5.2).

5.2. Phases at absolute zero temperature

In this subsection, phases at absolute zero temperature are investigated. Thanks to the formula

$$\lim_{T \rightarrow 0} \frac{\sinh(y/T)}{\cosh(y/T) + \cosh(x/T)} = \text{sgn}(y)\theta(|y| - |x|)$$

with the step function θ , the function $S(\bar{\Delta}, V, T)$ and the current at $T = 0$ are given by

$$S(\bar{\Delta}, V, 0) = -2 \int_{|\bar{\Delta}|}^{\hbar\omega_c} \frac{d\epsilon}{\sqrt{\epsilon^2 - \bar{\Delta}^2}} \theta\left(\epsilon - \left|\frac{eV}{2}\right|\right) , \quad (5.4)$$

$$\bar{J} = \frac{2G_0}{e} \text{sgn}(V) \int_{|\bar{\Delta}|}^{\hbar\omega_c} d\epsilon \frac{\sqrt{\epsilon^2 - \bar{\Delta}^2}}{\epsilon} \theta\left(\left|\frac{eV}{2}\right| - \epsilon\right) . \quad (5.5)$$

The stability index of the normal phase $\bar{\Delta} = 0$ is, then,

$$\chi_N = 1 + \lambda S(0, V, 0) = 2\lambda \ln \frac{|V|}{V_{10}} , \quad (5.6)$$

where V_{10} is defined by $V_{10} = \frac{2\hbar\omega_c}{e} \exp(-\frac{1}{2\lambda})$. Hence, the normal phase is stable if $|V| > V_{10}$ and unstable if $|V| < V_{10}$. As mentioned in the previous subsection, the average current is given by

$$\bar{J} = G_0 V . \quad (5.7)$$

For $|\bar{\Delta}| \geq |eV|/2$, (5.4) reduces to

$$S(\bar{\Delta}, V, 0) = -2 \int_{|\bar{\Delta}|}^{\hbar\omega_c} \frac{d\epsilon}{\sqrt{\epsilon^2 - \bar{\Delta}^2}} = -2 \cosh^{-1} \frac{\hbar\omega_c}{|\bar{\Delta}|} , \quad (5.8)$$

and (5.1) has a nontrivial solution,

$$|\bar{\Delta}| = \frac{\hbar\omega_c}{\cosh \frac{1}{2\lambda}} \equiv \Delta_0 , \quad (5.9)$$

irrespective of the bias voltage $|V| \leq V_{20} \equiv 2\Delta_0/e$. Its stability index at constant bias voltage is always positive:

$$\chi_V = \lambda \bar{\Delta} \left(\frac{\partial S}{\partial \bar{\Delta}} \right)_V = \frac{2\lambda \hbar \omega_c}{\sqrt{(\hbar \omega_c)^2 - |\bar{\Delta}|^2}} > 0. \quad (5.10)$$

In short, the ordered phase exists for $|V| \leq V_{20}$ and is stable at constant bias voltage. According to the inequality $\chi_I > \chi_V$ shown in Appendix E, this phase is also stable at constant current. Since the Fermi energies of the two reservoirs fall into the energy gap, the phase is insulating:

$$\bar{J} = 0. \quad (5.11)$$

Because of $V_{20}/V_{10} = 2/(1 + e^{-1/\lambda}) > 1$, there might be a first-order phase transition between the normal and insulating ($|\bar{\Delta}| = \Delta_0$) phases for $V_{10} < |V| < V_{20}$. This suggests the existence of another solution $|\bar{\Delta}|$ of (5.1) satisfying $0 < |\bar{\Delta}| < \Delta_0$. Indeed, for $|\bar{\Delta}| < |eV|/2$,

$$S(\bar{\Delta}, V, 0) = -2 \int_{|eV|/2}^{\hbar \omega_c} \frac{d\epsilon}{\sqrt{\epsilon^2 - \bar{\Delta}^2}} = -2 \left\{ \cosh^{-1} \frac{\hbar \omega_c}{|\bar{\Delta}|} - \cosh^{-1} \frac{|eV|}{2|\bar{\Delta}|} \right\}, \quad (5.12)$$

and thus (5.1) has a nontrivial solution for $V_{10} \leq |V| \leq V_{20}$:

$$|\bar{\Delta}| = \Delta_0 \sqrt{\frac{|V| - V_{10}}{V_{20} - V_{10}} \left\{ \frac{|V|}{V_{20}} + \frac{V_{10}(V_{20} - |V|)}{V_{20}(V_{20} - V_{10})} \right\}} \equiv \Delta_1(\lambda, V) (< \Delta_0). \quad (5.13)$$

This phase is unstable at constant bias voltage since the stability index is negative for $|\bar{\Delta}| < |eV|/2 < \hbar \omega_c$:

$$\chi_V = \lambda \bar{\Delta} \left(\frac{\partial S}{\partial \bar{\Delta}} \right)_V = \frac{2\lambda \hbar \omega_c}{\sqrt{(\hbar \omega_c)^2 - |\bar{\Delta}|^2}} - \frac{\lambda |eV|}{\sqrt{(eV)^2/4 - |\bar{\Delta}|^2}} < 0. \quad (5.14)$$

In contrast, *at constant current*, this phase is *stable* because the stability index is positive: $\chi_I > 0$ (for a proof, see Appendix E). In this case, the average current is given by

$$\begin{aligned} \bar{J} &= \frac{2G_0}{e} \text{sgn}(V) \int_{|\bar{\Delta}|}^{|eV|/2} d\epsilon \frac{\sqrt{\epsilon^2 - \bar{\Delta}^2}}{\epsilon} \\ &= \frac{2G_0}{e} |\bar{\Delta}| \text{sgn}(V) \left\{ \sqrt{\left(\frac{eV}{2\bar{\Delta}} \right)^2 - 1} - \tan^{-1} \sqrt{\left(\frac{eV}{2\bar{\Delta}} \right)^2 - 1} \right\} \equiv J_2(\lambda, V). \end{aligned} \quad (5.15)$$

These results are summarized in Figs. 1-4. At constant bias voltage (cf. Fig. 1), the insulating phase is stable up to the first threshold voltage eV_{10} , which is almost half of the zero-bias gap $2\Delta_0$ for small λ . Beyond the second threshold voltage eV_{20} which is equal to the zero-bias gap $2\Delta_0$, only the normal phase is stable. Between the two threshold voltages, i.e. $V_{10} \leq |V| \leq V_{20}$, both the insulating and normal phases

are stable, and a first-order phase transition between them is possible. Moreover, there exists an unstable phase separating the two stable ones, as shown by the dashed curve (i.e., the curve satisfying $|\overline{\Delta}| < e|V|/2$) in Fig. 1. The current-voltage characteristics are shown in Fig. 2. Note that the first-order transition corresponds to a sudden change in the current. The three regions discussed above are summarized in Table I.

On the other hand, at constant current (see Fig. 3), the unstable phase mentioned above is stabilized, and when one increases the current, a second-order phase transition to the normal phase occurs at the critical current $|\overline{J}| = J_{c0} \equiv G_0 V_{10}$. Near the critical current, the order parameter changes linearly with respect to the current:

$$|\overline{\Delta}| \simeq \frac{2\Delta_0}{\pi} \frac{J_{c0} - |\overline{J}|}{G_0 V_{20}}. \quad (5.16)$$

The corresponding voltage-current characteristics are shown in Fig. 4; a region $0 < \overline{J} < J_{c0}$ with negative differential conductivity appears.

The existence of negative differential conductivity can be understood as follows. When no bias voltage is applied, the system is in an insulating phase with an energy gap $2\Delta_0$, which is robust against low bias voltages. When the current starts to flow,

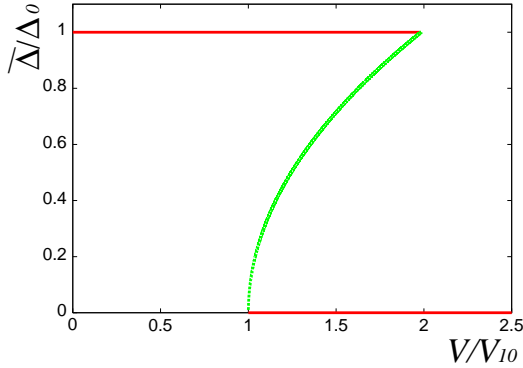


Fig. 1. Bias-voltage dependence of the order parameter at absolute zero temperature. In the constant-bias-voltage case, the solid lines correspond to the stable phases and the dashed curve to the unstable phase. All phases are stable in the constant-current case.

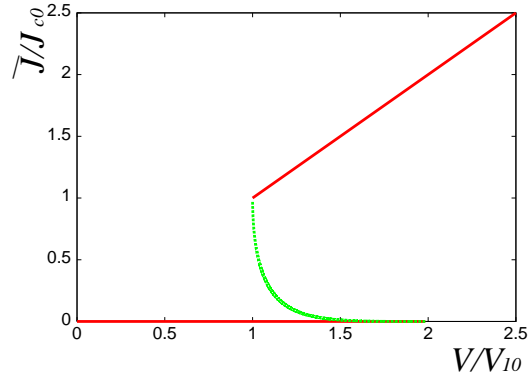


Fig. 2. Current versus bias voltage at absolute zero temperature. The solid lines and dashed curve correspond to those of Fig. 1.

Table I. Three regions at absolute zero temperature (constant-bias-voltage case)

	V	$ \overline{\Delta} $	\overline{J}
region A	$0 \leq V \leq V_{10}$	$\Delta_0(\lambda)$	0
region B	$V_{10} \leq V \leq V_{20}$	$0, \Delta_0(\lambda), \Delta_1(\lambda, V)$	$G_0 V, 0, J_2(\lambda, V)$
region C	$V_{20} < V$	0	$G_0 V$

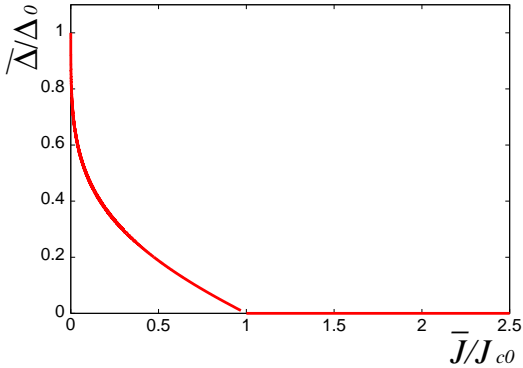


Fig. 3. Current dependence of the order parameter at absolute zero temperature. In the constant-current case, all phases are stable. Note that the point $(\bar{J}, |\bar{\Delta}|) = (0, \Delta_0)$ corresponds to the insulating phases for $V_{10} \leq |V| \leq V_{20}$.

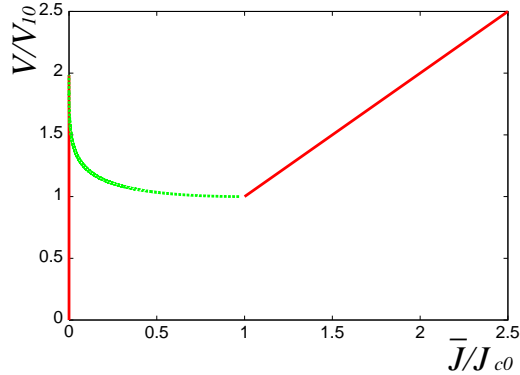


Fig. 4. Bias voltage versus current at absolute zero temperature (constant current). The curve is essentially the same as Fig. 2. Only stabilities are different.

electrons with energy larger than the gap should exist, and the bias voltage should be on the order of the zero-bias gap: $|V| \sim 2\Delta_0/e$. At the same time, the gap is reduced by the existence of the current. As the current increases, the gap $2|\bar{\Delta}|$ is reduced further, and the corresponding bias voltage $|V| \sim 2|\bar{\Delta}|/e$ becomes smaller. Thus, negative differential conductivity does appear. When the current reaches the critical current, the gap disappears and the phase becomes normal. As the normal-phase conductivity is positive, negative differential conductivity appears only up to the critical current: $|\bar{J}| < J_{c0}$.

5.3. Phases at finite temperature at constant bias voltage

In this subsection, we investigate the finite-temperature phases at constant bias voltage.

(A) Phase Diagram

Let us begin with the investigation of the phase diagram. As in the zero-temperature case, three regions exist in the VT -plane; one with a unique stable ordered phase (region A), one where ordered and normal phases are stable (region B) and one with the normal phase (region C). The three regions are depicted in Fig. 5. The boundary curve between region A and the others is implicitly given by

$$0 = \frac{\chi_N}{2\lambda} = \frac{1}{2\lambda} + \frac{1}{2}S(0, V, T) = \frac{1}{2\lambda} - \int_0^{\hbar\omega_c/T} \frac{d\epsilon}{\epsilon} \frac{\sinh \epsilon}{\cosh(\frac{eV}{2T}) + \cosh \epsilon},$$

where χ_N is the stability index of the normal phase. When terms on the order of $\exp\{-(2\hbar\omega_c - e|V|)/(2T)\}$ are neglected, it reduces to

$$\log \frac{eV_{10}}{2T} = \int_0^\infty d\epsilon \log \epsilon \frac{\cosh(\frac{eV}{2T}) \cosh \epsilon + 1}{(\cosh(\frac{eV}{2T}) + \cosh \epsilon)^2} \equiv \phi\left(\frac{eV}{2T}\right), \quad (5.17)$$

where the function ϕ is defined by the integral of the middle term. When $V = 0$, (5.17) leads to

$$\log \frac{eV_{10}}{2T} = \int_0^\infty d\epsilon \frac{\log \epsilon}{1 + \cosh \epsilon} = -\log \frac{2e^\gamma}{\pi} \quad \text{or} \quad T = T_{c0} \equiv \frac{e^\gamma}{\pi} eV_{10}, \quad (5.18)$$

where γ is the Euler constant and T_{c0} corresponds to the transition temperature at zero bias voltage. Then, (5.17) reads

$$\log \left(\frac{\pi}{2e^\gamma} \frac{T_{c0}}{T} \right) = \phi \left(\frac{\pi}{2e^\gamma} \frac{V}{V_{10}} \frac{T_{c0}}{T} \right). \quad (5.19)$$

This implies that the boundary between region A and the others is independent of the coupling constant once it is plotted in terms of V/V_{10} and T/T_{c0} (cf. the solid curve in Fig. 5). We note that the boundary curve (5.19) can be expressed as $|V| = V_1(T)$ in terms of a single-valued function $V_1(T)$ of T , which will be referred to as the first threshold voltage.

The phase boundary curve (5.19) indicates the bias-induced decrease of the transition temperature for low $|V|$ and the temperature-induced increase of the first threshold voltage for low T . Indeed, for $e|V| \ll T$, with the aid of the formula $\phi'(0) = 0$ and

$$\phi''(0) = \int_0^\infty d\epsilon \frac{\log \epsilon (\cosh \epsilon - 2)}{(1 + \cosh \epsilon)^2} = \frac{7\zeta(3)}{2\pi^2},$$

(5.19) reduces to

$$T \equiv T_c(V) = T_{c0} \exp \left[-\frac{7\zeta(3)}{16e^{2\gamma}} \left(\frac{VT_{c0}}{V_{10}T} \right)^2 \right] \simeq T_{c0} \left\{ 1 - \frac{7\zeta(3)}{16e^{2\gamma}} \left(\frac{V}{V_{10}} \right)^2 \right\}, \quad (5.20)$$

where $\zeta(n)$ is the Riemann zeta function. Thus, the transition temperature $T_c(V)$ decreases with the bias voltage V . On the other hand, when $T \ll e|V|$, one may apply the standard technique of evaluating the low-temperature properties of the free fermion gas, and we have

$$\begin{aligned} \phi \left(\frac{eV}{2T} \right) &= - \int_0^\infty d\epsilon \log \left(\frac{\epsilon}{2T} \right) \frac{d}{d\epsilon} \left[\frac{1}{e^{(\epsilon-eV)/(2T)} + 1} + \frac{1}{e^{(\epsilon+eV)/(2T)} + 1} \right] \\ &\simeq \log \frac{e|V|}{2T} - \frac{2\pi^2}{3} \left(\frac{T}{eV} \right)^2 = \log \frac{e|V|}{2T} - \frac{2e^{2\gamma}}{3} \left(\frac{TV_{10}}{T_{c0}V} \right)^2, \end{aligned} \quad (5.21)$$

up to T^2 . Thus, the first threshold voltage $V_1(T)$ near absolute zero temperature is given by

$$|V| = V_1(T) \simeq V_{10} \exp \left[\frac{2e^{2\gamma}}{3} \left(\frac{TV_{10}}{T_{c0}V_1} \right)^2 \right] \simeq V_{10} \left\{ 1 + \frac{2e^{2\gamma}}{3} \left(\frac{T}{T_{c0}} \right)^2 \right\}, \quad (5.22)$$

which shows that the first threshold voltage increases as temperature increases. Careful asymptotic analysis indicates that $T/(e|V|) \sim 0.05$ is the upper bound where the estimation (5.22) is valid.

On the other hand, the boundary curve $|V| = V_2(T)$ between regions B and C (the dashed curve in Fig. 5) is derived by solving the self-consistent equation (5.1)

for nonvanishing order parameters. It starts from the point $(|V|, T) = (V_{20}, 0)$ and terminates at a point P on the boundary curve $|V| = V_1(T)$ between region A and the others (see Fig. 5). The behaviour near the terminating point P can be investigated on the basis of the Ginzburg-Landau expansion of the self-consistent equation (5.1). Up to $\overline{\Delta}^4$, the self-consistent equation becomes

$$\frac{K_2}{2} \left(\frac{\overline{\Delta}}{T} \right)^2 - \frac{K_4}{8} \left(\frac{\overline{\Delta}}{T} \right)^4 = \frac{\chi_N}{2\lambda}, \quad (5.23)$$

where $\chi_N = 1 + \lambda S(0, V, T)$ is the stability index of the normal phase, and the coefficients K_2 and K_4 depend only on the ratio V/T (their concrete expressions are given in Appendix F). As V/T increases, K_2 changes sign from minus to plus at $V/T \simeq 2.1865 \times V_{10}/T_{c0}$ and K_4 is positive there. Hence, when $K_2 < 0$, the quartic polynomial in the left-hand side of (5.23) has one maximum value 0 at $|\overline{\Delta}| = 0$. In this case, when $\chi_N > 0$, (5.23) has no solution (region C), and when $\chi_N < 0$, (5.23) has one nonvanishing solution in $|\overline{\Delta}|$ (region A). On the other hand, when $K_2 > 0$, the quartic polynomial in the left-hand side of (5.23) has a local minimum 0 at $|\overline{\Delta}| = 0$, and a local maximum $K_2^2/(2K_4)$ at $|\overline{\Delta}| = T\sqrt{2K_2/K_4}$. Then, with respect to $|\overline{\Delta}|$, (5.23) has no solution when $K_2^2/(2K_4) < \chi_N/(2\lambda)$ (region C), two nonvanishing solutions when $K_2^2/(2K_4) > \chi_N/(2\lambda) > 0$ (region B) and one nonvanishing solution when $\chi_N/(2\lambda) < 0$ (region A). Therefore, the boundary curve $|V| = V_2(T)$ near point P is given by $K_2^2/(2K_4) = \chi_N/(2\lambda)$. Then, since the curve $|V| = V_1(T)$ corresponds to $\chi_N = 0$, the simultaneous solution of (5.19) and $K_2 = 0$ is the terminating point P: $T \equiv T^* \simeq 0.5571 \times T_{c0}$ and $|V| \simeq 1.2181 \times V_{10}$. Note that, in contrast to the first-threshold-voltage curve $|V|/V_{10} = V_1(T)/V_{10}$, the curve $|V|/V_{10} = V_2(T)/V_{10}$ depends not only on T/T_{c0} but also on λ (cf. Fig. 5).

(B) Order Parameter

Both the bias-voltage dependence of the order parameter and the current-voltage characteristics change continuously from those at zero temperature $T = 0$ as shown in Figs. 6-9 for $1/\lambda = 4.8$. When temperature is less than T^* corresponding to the point P of Fig. 5, a voltage range $V_1(T) < |V| < V_2(T)$ exists where the order

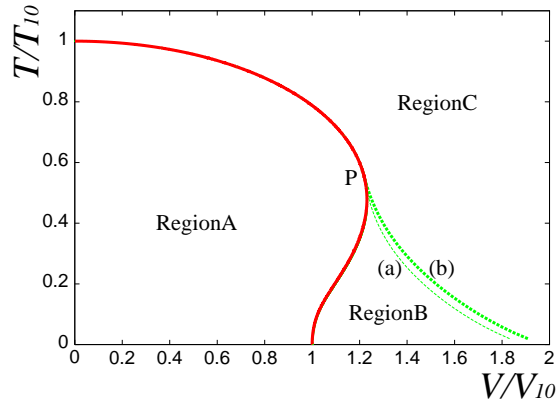


Fig. 5. Phase diagram at constant bias voltage. A unique stable ordered phase occurs in region A, one stable ordered phase and the normal phase in region B and only the normal phase in region C. The solid curve represents the second-order phase transition, and the dashed curves represent the first-order phase transition. For comparison, the phase transition curve for (a) $\lambda = 4.8$ is shown together with that for (b) $\lambda = 3.0$.

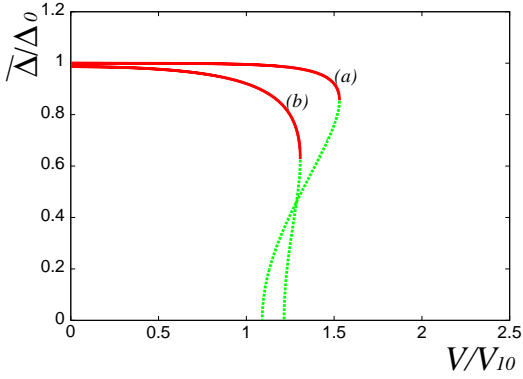


Fig. 6. The order parameter versus bias voltage for (a) $T = 0.01 \exp(-1/2\lambda)|eV_{10}|$ ($= 0.194T_{c0}$) and (b) $T = 0.02 \exp(1/2\lambda)|eV_{10}|$ ($= 0.389T_{c0}$). The solid lines correspond to the stable phase, and the dashed lines correspond to the unstable phase.

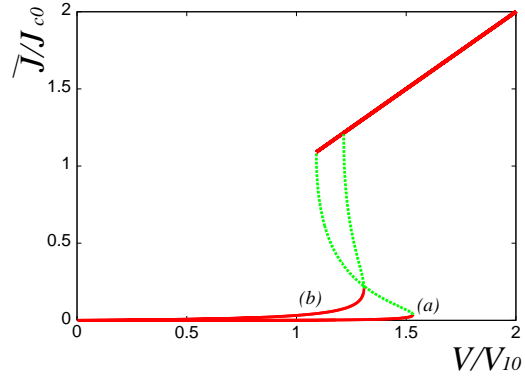


Fig. 7. Current versus bias voltage for (a) $T = 0.01 \exp(1/2\lambda)|eV_{10}|$ ($= 0.194T_{c0}$) and (b) $T = 0.02 \exp(1/2\lambda)|eV_{10}|$ ($= 0.389T_{c0}$). The solid lines correspond to the stable phase, and the dashed lines correspond to the unstable phase.

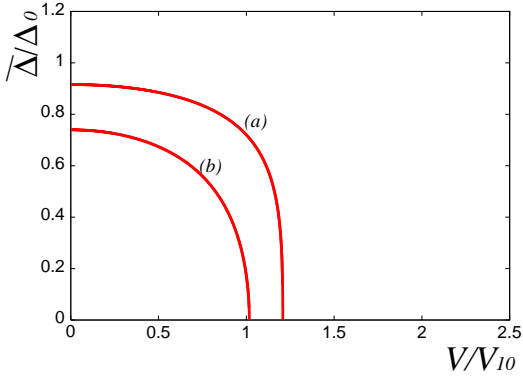


Fig. 8. The order parameter versus bias voltage for (a) $T = 0.03 \exp(1/2\lambda)|eV_{10}|$ ($= 0.583T_{c0}$) and (b) $T = 0.04 \exp(1/2\lambda)|eV_{10}|$ ($= 0.778T_{c0}$). All phases shown in this figure are stable.

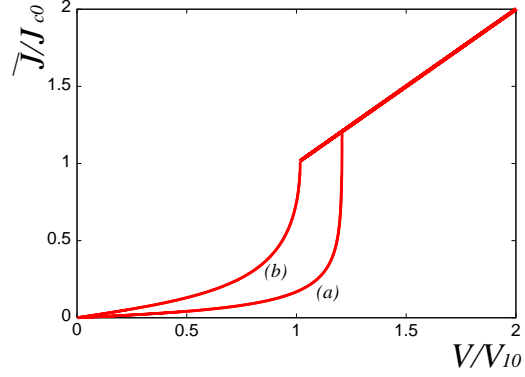


Fig. 9. Current versus bias voltage for (a) $T = 0.03 \exp(1/2\lambda)|eV_{10}|$ ($= 0.583T_{c0}$) and (b) $T = 0.04 \exp(1/2\lambda)|eV_{10}|$ ($= 0.778T_{c0}$). All phases shown in this figure are stable.

parameter is a triple-valued function of the bias voltage $|V|$ (see Fig. 6) with an unstable middle branch and, hence, where the first-order phase transition is possible. The corresponding current-voltage characteristics are S-shaped, as shown in Fig. 7. Note that the small current observed at low bias voltage is due to thermally activated carriers. On the other hand, when the temperature is higher than T^* , the unstable branch disappears and the order parameter becomes a single-valued function of the bias voltage (see Fig. 8). In this case, the current is a monotonically increasing function of the bias voltage (see Fig. 9).

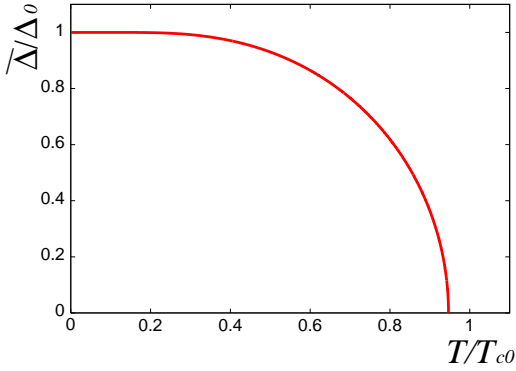


Fig. 10. The order parameter versus temperature for $V = 0.551V_{10}$. The solid lines correspond to the stable phase and the dashed lines correspond to the unstable phase.

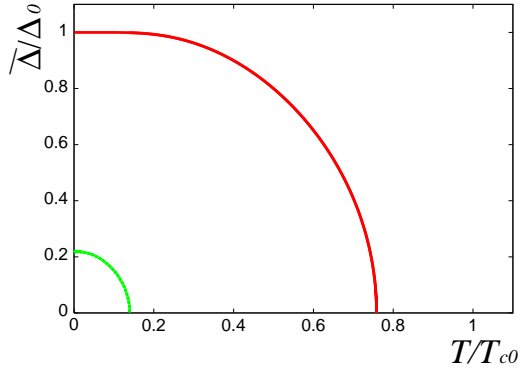


Fig. 11. The order parameter versus temperature for $V = 1.047V_{10}$. The solid lines correspond to the stable phase and the dashed lines correspond to the unstable phase.

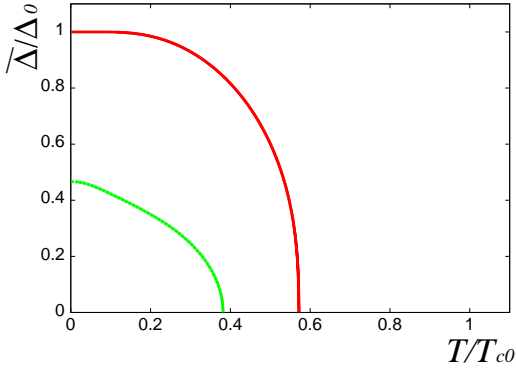


Fig. 12. The order parameter versus temperature for $V = 1.213V_{10}$. The solid lines correspond to the stable phase and the dashed lines correspond to the unstable phase.

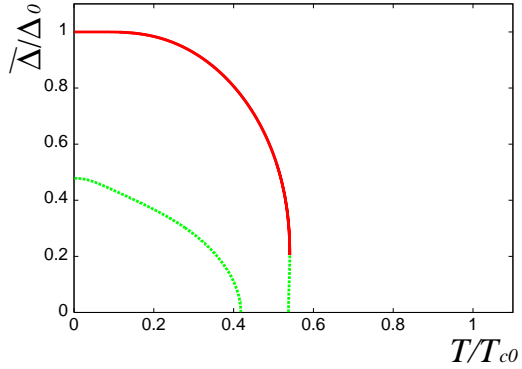


Fig. 13. The order parameter versus temperature for $V = 1.224V_{10}$. The solid lines correspond to the stable phase and the dashed lines correspond to the unstable phase.

The temperature dependence of the order parameter at constant bias voltage is shown in Figs. 10-15. At low bias voltage, the temperature dependence of the order parameter is similar to that in the absence of the bias (see Fig. 10). As the bias voltage increases, a lower-temperature branch corresponding to the unstable phase appears (see Fig. 11). In the temperature range where the unstable phase appears, the normal phase is stable in the sense of $\chi_N > 0$, and the first-order phase transition between the stable ordered and normal phases is possible. As the bias voltage increases further, the unstable branch approaches the stable branch and the two branches join (Figs. 12-14). Note that an unstable portion appears in the outer curve of Fig. 13. This is because the temperature T^* is higher than the temperature where $\frac{dV_1(T)}{dT} = 0$. For higher bias voltage, the stable ordered phase always co-exists with the normal phase, and the region where they co-exist shrinks with increasing bias voltage (see Figs. 14 and 15). We re-

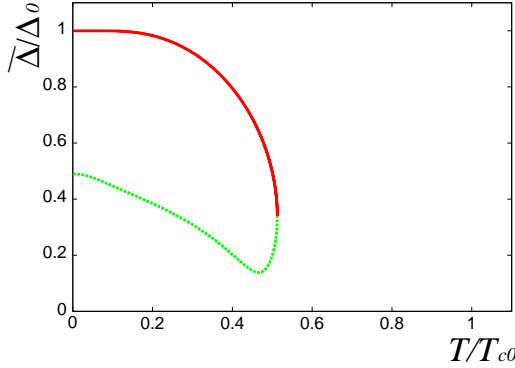


Fig. 14. The order parameter as a function of temperature for $V = 1.235V_{10}$. The solid lines and dashed lines in this figure have the same meaning as those in Figs. 6 and Fig. 7.

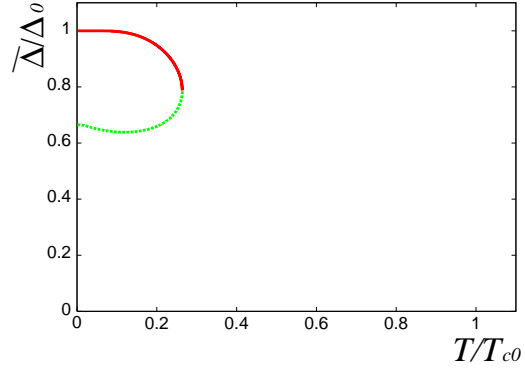


Fig. 15. The order parameter as a function of temperature for $V = 1.433V_{10}$. The solid lines and dashed lines in this figure have the same meaning as those in Figs. 6 and Fig. 7.

mark that both the phase diagram (Fig. 5) and the temperature dependence of the order parameter (Figs. 14 and 15) are similar to those for the nonequilibrium superconducting phase induced by excess quasiparticles, which was studied by Scalapino *et al.*^{32),33)} This will be discussed in more detail in the last section.

5.4. Phases at finite temperature at constant current

(A) Phase Diagram

As in the zero-temperature case, at constant current, all the nontrivial solutions are stable in the sense of $\chi_I > 0$, and the properties are drastically changed from those at constant bias voltage. First, only the ordered and normal phases exist and the phase transition between the two is always of second order. The corresponding boundary curve is given by (5.19):

$$\log\left(\frac{\pi T_{c0}}{2e\gamma T}\right) = \phi\left(\frac{\pi T_{c0}\bar{J}}{2e\gamma J_{c0}T}\right), \quad (5.24)$$

where J_{c0} is the zero-temperature threshold current defined just above (5.16) (Fig. 16). From (5.24), the critical temperature $T_c(\bar{J})$ for small current and the threshold current $J_c(T)$ at low temperature

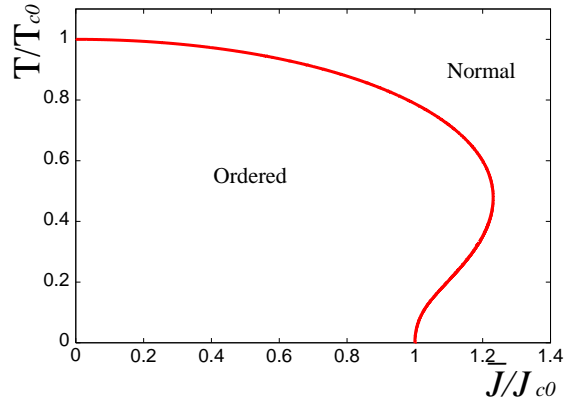


Fig. 16. Phase diagram at constant current. Only the second-order phase transition occurs at constant current.

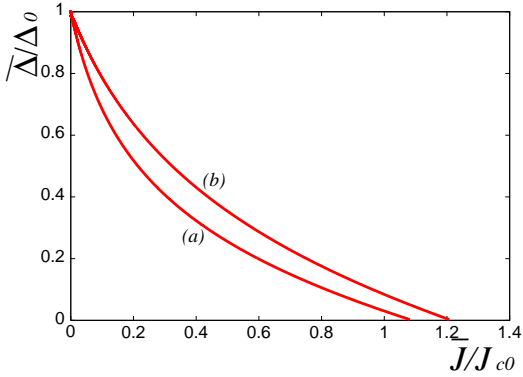


Fig. 17. The order parameter versus current for (a) $T = 0.01 \exp(1/2\lambda)|eV_{10}|$ ($= 0.194T_{c0}$) and (b) $T = 0.02 \exp(1/2\lambda)|eV_{10}|$ ($= 0.389T_{c0}$). All phases shown in this figure are stable under constant current.

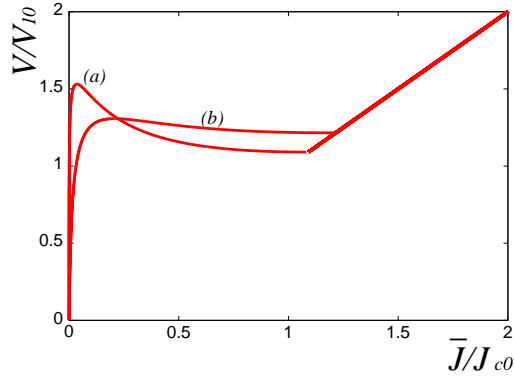


Fig. 18. Current versus bias voltage for (a) $T = 0.01 \exp(1/2\lambda)|eV_{10}|$ ($= 0.194T_{c0}$) and (b) $T = 0.02 \exp(1/2\lambda)|eV_{10}|$ ($= 0.389T_{c0}$). All phases shown in this figure are stable under constant current.

are found to be

$$T \equiv T_c(\bar{J}) \simeq T_{c0} \left\{ 1 - \frac{7\zeta(3)}{16e^{2\gamma}} \left(\frac{\bar{J}}{J_{c0}} \right)^2 \right\} \quad (5.25)$$

and

$$|\bar{J}| \equiv J_c(T) \simeq J_{c0} \left\{ 1 + \frac{2e^{2\gamma}}{3} \left(\frac{T}{T_{c0}} \right)^2 \right\}. \quad (5.26)$$

The difference between the phase diagram at constant bias voltage and that at constant current can be understood as follows. Since a larger order parameter implies a smaller current, the nontrivial phase with larger order parameter in region B of Fig. 5 corresponds to the phase with smaller current. As a result, the phase diagram in Fig. 16 does not have a region where more than one phase is stable.

(B) Order Parameter

As before, when temperature increases, both the current dependence of the order parameter and the voltage-current characteristics change continuously from those at zero temperature. At any temperature, the order parameter is a monotonically decreasing function of the current (cf. Figs. 17 and 19). For $|\bar{J}| \sim 0$, the decrease in the order parameter is found to be proportional to the squared current, but the quadratic region is not visible at lower temperature $T \leq 0.6 \times T_{c0} \simeq T^*$, where the decrease in the order parameter is approximately proportional to the current. The corresponding voltage-current characteristics behave as shown in Figs. 18 and 20. We remark that negative differential conductivity appears only at temperatures lower than T^* , and otherwise the differential conductivity is positive.

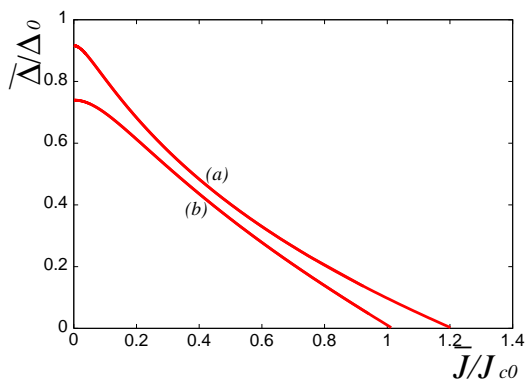


Fig. 19. The order parameter versus current for (a) $T = 0.03 \exp(1/2\lambda)|eV_{10}|$ ($= 0.583T_{c0}$) and (b) $T = 0.04 \exp(1/2\lambda)|eV_{10}|$ ($= 0.778T_{c0}$). All phases shown in this figure are stable under constant current.

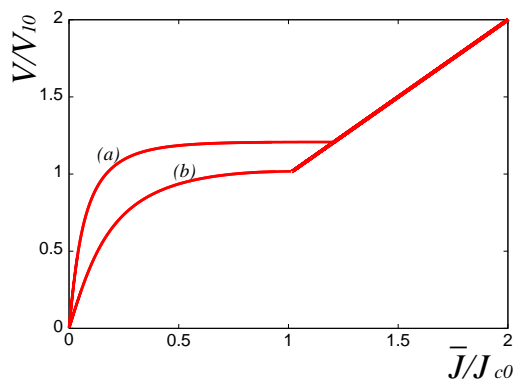


Fig. 20. Current versus bias voltage for (a) $T = 0.03 \exp(1/2\lambda)|eV_{10}|$ ($= 0.583T_{c0}$) and (b) $T = 0.04 \exp(1/2\lambda)|eV_{10}|$ ($= 0.778T_{c0}$). All phases shown in this figure are stable under constant current.

The temperature dependence of the order parameter at constant current is shown in Fig. 21. The order parameter is reduced by the presence of the current. Even for a smaller current (see the cases $\bar{J}/J_{c0} = 0.3$ and 0.6 in Fig. 21), the lower-temperature part is more suppressed than the higher-temperature part. At the threshold current $\bar{J} = J_{c0}$, the order parameter at zero temperature vanishes (see the case $\bar{J}/J_{c0} = 0.95$ in Fig. 21). When the current exceeds the threshold, re-entrance to the normal phase appears at low temperature. As the current increases, the temperature range with nonvanishing order parameter shrinks and eventually vanishes (see the case $\bar{J}/J_{c0} = 1.10$ in Fig. 21).

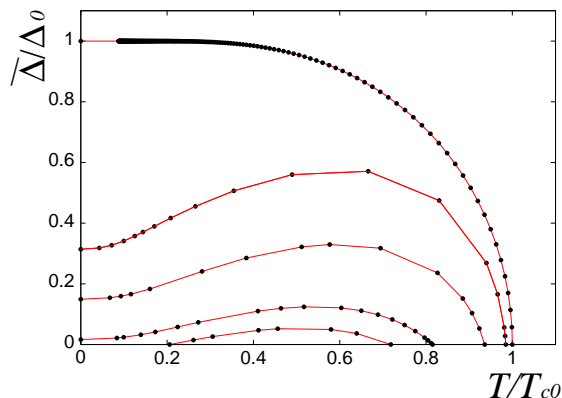


Fig. 21. The order parameter as a function of temperature for $\bar{J}/J_{c0} = 0, 0.3, 0.6, 0.95,$ and 1.10 from top to bottom. To draw this figure, we use an approximate equation of (5-1) similar to (5-17). For computational reasons, the numbers of data are limited for $\bar{J}/J_{c0} = 0.3, 0.6, 0.95$ and 1.10 .

§6. Summary and Discussions

We have studied the nonequilibrium Peierls transition in a TLM chain connected to two reservoirs at different chemical potentials (their difference corresponds to the

bias voltage) by combining a mean-field approximation and formula (1.1), which characterizes a nonequilibrium steady state and is an outcome of the algebraic field-theoretical approach to nonequilibrium statistical mechanics. The averaged lattice distortion serves as an order parameter, and its self-consistent equation is obtained by averaging the equation of motion of the lattice distortion with respect to a nonequilibrium steady state. When the bias voltage and temperature are chosen as control parameters, three parameter regions are distinguished: region A where a single stable ordered phase is possible, region B where stable normal, stable ordered, and unstable ordered phases are possible and region C where only the stable normal phase is possible (cf. Fig. 5). The transition between regions A and C is of second order, and the transition temperature decreases with increasing bias voltage. A first-order phase transition between normal and ordered phases may occur in region B. In regions A and C, the current is a single-valued function of the bias voltage, and in region B, the current-voltage characteristics are S-shaped (i.e. negative differential conductivity exists). In contrast, when the current and temperature are chosen as control parameters, all the nontrivial solutions of the self-consistent equation become stable in the sense of linear stability. The phase transition between the ordered and normal phases is always of second order, and re-entrant behaviour is seen for currents larger than the threshold value, J_{c0} . Negative differential conductivity appears only when the temperature is lower than a certain value T^* . We remark that, as in the equilibrium case,³⁴⁾ the mean field approach is expected to provide a qualitatively correct description of the nonequilibrium phase transition in quasi-1D systems, although the 1D order may be destroyed by fluctuations.

As mentioned in the previous section, the phase diagram, particularly the possibility of the re-entrant behaviour, and the temperature dependence of the order parameter at higher bias voltage are similar to those of the nonequilibrium superconducting phase induced by excess quasiparticles, which were studied by Scalapino *et al.*^{32),33)} This can be understood because of the similarity between the self-consistent equations in the two cases. Indeed, let E be $\sqrt{\epsilon^2 + \bar{\Delta}^2}$, then the self-consistent equation (5.1) is rewritten as

$$\frac{1}{\lambda} = \int_{-\hbar\omega_c}^{\hbar\omega_c} \frac{d\epsilon}{E} \left\{ \tanh \frac{1}{2T} \left(E - \frac{eV}{2} \right) + \tanh \frac{1}{2T} \left(E + \frac{eV}{2} \right) \right\}, \quad (6.1)$$

which reduces to the self-consistent equation of Scalapino *et al.* [cf. Eq.(6) of Ref. 32)] if the second term is dropped and $eV/2$ is replaced with the effective chemical potential μ^* . In view of this similarity, one can interpret the suppression of the charge-density-wave order induced by the bias voltage (equivalently by the current) as being due to excess electrons coming from the two reservoirs. However, since the two self-consistent equations are not exactly the same, the two systems are different in their properties at lower bias voltage (namely, in the temperature dependence of the order parameter and the possibility of the second-order phase transition).

As is well known, systems with density waves may exhibit nonlinear conduction due to density-wave sliding.³⁴⁾ On the other hand, because of the above observation and the similarity between the mean-field approximation for superconductors and

that for density waves, the current-induced suppression of order discussed here is generally expected for systems with density waves. However, except for cases where density waves are strongly pinned, the current-induced suppression of order may not be observed because it is related to the amplitude degrees of freedom, while the sliding is related to the easily excitable phase degrees of freedom.

We remark that the mean-field approximation of the TLM chain is equivalent to the mean-field approximation of the half-filled charge order in the spinless extended Hubbard chain, the Hamiltonian of which is given by

$$H_{\text{CO}} = -t_0 \sum_{j=0}^{L-1} \{C_{j+1}^\dagger C_j + C_j^\dagger C_{j+1}\} + U \sum_{j=0}^{L-1} n_{j+1} n_j - U \sum_{j=0}^L n_j, \quad (6.2)$$

where $n_j = C_j^\dagger C_j$ is the number operator of the spinless fermions at site j . Indeed, in the continuum limit discussed in Appendix A [cf. (A.2)], the mean-field equations become (3.2) and (3.13) with replacement $\sigma_x \rightarrow \sigma_z$ and $\lambda \rightarrow U/(\pi t_0)$, where the order parameter is proportional to the charge disproportion between even and odd sites. Hence, as in the open TLM chain, the charge order in the open extended Hubbard chain is suppressed by current. This observation suggests that current-induced suppression could be a possible origin of the nonlinear conduction, which is different from phenomena such as sliding density waves,³⁴⁾ strong impurity scattering in a Tomonaga-Luttinger liquid,²⁹⁾ dielectric breakdown of Mott insulators³⁰⁾ or the Kosterlitz-Thouless transition.³⁵⁾

It is then interesting to compare the present results with the experiments by Terasaki and his co-workers^{24), 25), 26), 27)} on the charge order in the organic conductors θ -(BEDT-TTF)₂CsM(SCN)₄ ($M = \text{Zn, Co, Co}_{0.7}\text{Zn}_{0.3}$). The existence of hysteresis and spontaneous oscillation at constant bias voltage and negative differential conductivity at constant current reported in Ref. 25) is consistent with the present results. In Ref. 27), it was shown that the current-induced decrease in the order parameter is proportional to the current and, this observation agrees with the current dependence of the order parameter at temperatures where nonlinear conduction is possible (cf. Figs. 17 and 19). Also, according to the present analysis, negative differential conductivity appears only when $\lambda \sim U/(\pi t_0)$ is not too large. This seems to imply that systems with weaker charge ordering are more favourable for negative differential conductivity, and further imply that, because of the fragility of their charge order, the organic conductors mentioned above would be such systems. Moreover, in these materials, the charge order has no long-range order in the phase mode, and thus excitations in the amplitude mode instead of charge-order sliding would be responsible for nonlinear conductivity. These observations suggest that current-induced suppression of the charge order is the origin of the phenomena investigated by Terasaki and co-workers.^{24), 25), 26), 27)} More quantitative analysis based on a realistic model of the organic conductors will be studied elsewhere.

Moreover, since the extended Hubbard model (6.2) is a typical model of strongly correlated systems, the present analysis would provide some insight into the negative differential conductivity recently reported in strongly correlated systems.^{29), 30), 28), 31)} In particular, as the extended Hubbard chain (6.2) is equivalent to the XXZ chain

via the Jordan-Wigner transformation, the negative differential conductivity in the nonequilibrium XXZ model found by Benenti *et al.*²⁸⁾ should be approximately understood in terms of the present results. However, further investigation is necessary because in the work of Benenti *et al.*, the system is driven to a nonequilibrium steady state by stochastic activation of the boundary spins, not through coupling with infinitely extended reservoirs.

Acknowledgements

The authors thank T. Prosen, G. Benenti, G. Casati, Y. Matsunaga, Baowen Li, Bambi Hu, K. Nakamura, A. Sugita for fruitful discussions. This work is partially supported by a Grant-in-Aid for Scientific Research (Nos. 17340114, 16076213, and 17540365) from the Japan Society of the Promotion of Science, for the ‘‘Academic Frontier’’ Project at Waseda University and the 21st Century COE Program at Waseda University ‘‘Holistic Research and Education Center for Physics of Self-organization Systems’’ both from the Ministry of Education, Culture, Sports, Science and Technology of Japan.

Appendix A

— Derivation of a continuous model —

In this appendix, we derive the continuous open TLM model from the discrete open SSH model. Hamiltonian of our system is consist of the SSH part (H_S), two reservoirs (H_B), and the interaction between SSH part and reservoirs (V):

$$\begin{aligned}
 H &= H_S + V + H_B \\
 H_S &= - \sum_{\sigma} \sum_{n=-1}^{L+1} \left(t_{n+1,n} C_{n+1\sigma}^{\dagger} C_{n\sigma} + (\text{h.c.}) \right) + \frac{K}{2} \sum_{n=-1}^L (y_{n+1} - y_n)^2 + \frac{M}{2} \sum_{n=0}^L \dot{y}_n^2 \\
 V &= \sum_{\sigma} \int dk \hbar \left(\bar{v}_k C_{0\sigma}^{\dagger} a_{k\sigma} + \bar{w}_k C_{L\sigma}^{\dagger} b_{k\sigma} + (\text{h.c.}) \right), \\
 H_B &= \sum_{\sigma} \int dk \left(\hbar\omega_{kL} a_{k\sigma}^{\dagger} a_{k\sigma} + \hbar\omega_{kR} b_{k\sigma}^{\dagger} b_{k\sigma} \right), \tag{A.1}
 \end{aligned}$$

where $C_{n\sigma}$ denotes the annihilation operator of an electron at the n th site with spin σ (cf. $C_{-1\sigma} \equiv 0$, $C_{L+1\sigma} \equiv 0$), $a_{k\sigma}$ ($b_{k\sigma}$) denotes the annihilation operator of the left (right) reservoir with wave number k and spin σ , and y_n denotes a lattice displacement of the n th site, respectively. Su, Schrieffer, and Heeger²³⁾ assumed that $t_{n+1,n}$ is a linear function of the lattice displacement:

$$t_{n+1,n} \equiv t_0 - \alpha(y_{n+1} - y_n).$$

Takayama *et al.*²²⁾ approximated the dispersion relation of electrons as $-2t_0 \cos[(k \pm k_F)a] \approx \pm v_f k$, and introduced the left/right moving electron fields $\psi_{L\sigma}(2na)/\psi_{R\sigma}(2na)$, and $\Delta(na) = (-1)^n 4\alpha y_n$ with a the lattice constant. Then, by assuming $L \equiv -1$

(mod 4) and considering a to be very small, the discrete Hamiltonian (A.1) reads as

$$\begin{aligned}
H_S^{(e)} &\simeq \sum_{\sigma} \int_0^l dx \left(\psi_{L\sigma}^{\dagger}(x), \psi_{R\sigma}^{\dagger}(x) \right) \left[-2iat_0\sigma_y \frac{\partial}{\partial x} + \sigma_x \Delta(x) \right] \begin{pmatrix} \psi_{L\sigma}(x) \\ \psi_{R\sigma}(x) \end{pmatrix} \\
H_S^{(\text{ph})} &\simeq \frac{K}{8\alpha^2 a} \int_0^l dx \Delta(x)^2 + \int_0^l dx \frac{M}{32\alpha^2 a} \dot{\Delta}(x)^2 \\
V &\simeq \sqrt{a} \sum_{\sigma} \int dk \hbar \left[\bar{v}_k \left(-i\psi_{L\sigma}^{\dagger}(a) + \psi_{R\sigma}^{\dagger}(a) \right) a_{k\sigma} + \bar{w}_k \left(\psi_{L\sigma}^{\dagger}(l) - i\psi_{R\sigma}^{\dagger}(l) \right) b_{k\sigma} \right] + (h.c.) \\
H_B &= \sum_{\sigma} \int dk \left(\hbar\omega_{kL} a_{k\sigma}^{\dagger} a_{k\sigma} + \hbar\omega_{kR} b_{k\sigma}^{\dagger} b_{k\sigma} \right).
\end{aligned}$$

Moreover, $C_{-1\sigma} \equiv 0$ and $C_{L+1\sigma} \equiv 0$ lead to

$$\psi_{L\sigma}(0) + i\psi_{R\sigma}(0) = 0, \quad i\psi_{L\sigma}(l) + \psi_{R\sigma}(l) = 0,$$

where ℓ is defined by $\ell = a + La$. We remark that case of $L \equiv +1 \pmod{4}$ leads to essentially the same results. To make the boundary condition simpler, we introduce $d_{\sigma}(x)$ and $e_{\sigma}(x)$ by

$$\begin{aligned}
C_{2n-1\sigma} &= (-1)^n \sqrt{2a} d_{\sigma}(2na) = (-1)^n \sqrt{a} [\psi_{L\sigma}(2na) + i\psi_{R\sigma}(2na)] \\
C_{2n\sigma} &= (-1)^n \sqrt{2a} e_{\sigma}(2na) = (-1)^n \sqrt{a} [i\psi_{L\sigma}(2na) + \psi_{R\sigma}(2na)]. \quad (\text{A}\cdot 2)
\end{aligned}$$

By using these fields, the momentum $\Pi(x) \equiv \dot{\Delta}(x)$ conjugate to $\Delta(x)$, the Fermi velocity $v \equiv 2at_0/\hbar$, dimensionless coupling constant $\lambda \equiv 4\alpha^2 a/\pi\hbar vK$, phonon frequency $\omega_0 \equiv \sqrt{4K/M}$, and the matrix elements $v_k \equiv \sqrt{2a}\bar{v}_k$ and $w_k \equiv \sqrt{2a}\bar{w}_k$, the Hamiltonians (2.2), (2.7), and (2.8), and the boundary condition (2.5) in §2 are obtained.

Appendix B

Normal modes

In this appendix, we derive normal modes of the mean-field Hamiltonian H_{MF} . Let $\{\phi_{\lambda}(x)\}_{\lambda}$ be a complete orthonormal solution of the eigenvalue problem:

$$\left[-i\hbar v\sigma_y \frac{\partial}{\partial x} + \Delta(x)\sigma_x \right] \phi_{\lambda}(x) = \hbar\epsilon_{\lambda}\phi_{\lambda}(x), \quad (\text{B}\cdot 1)$$

$$\phi_{\lambda}(x) \equiv \begin{pmatrix} \phi_{\lambda}^{+}(x) \\ \phi_{\lambda}^{-}(x) \end{pmatrix}, \quad \phi_{\lambda}^{+}(0) = 0, \quad \phi_{\lambda}^{-}(\ell) = 0, \quad (\text{B}\cdot 2)$$

and we expand the electron field

$$\Psi_{\sigma}(x) = \begin{pmatrix} d_{\sigma}(x) \\ e_{\sigma}(x) \end{pmatrix} = \sum_{\lambda,\sigma} \phi_{\lambda}(x) f_{\lambda\sigma}, \quad (\text{B}\cdot 3)$$

where $\{f_{\lambda\sigma}, f_{\lambda'\sigma'}^{\dagger}\} = \delta_{\lambda,\lambda'}\delta_{\sigma,\sigma'}$. In terms of $f_{\lambda\sigma}$, the mean-field Hamiltonian reads

$$\frac{1}{\hbar} H_{\text{MF}} = \sum_{\lambda,\sigma} \epsilon_{\lambda} f_{\lambda\sigma}^{\dagger} f_{\lambda\sigma} + \int d\mathbf{k} \left(\omega_{kL} a_{\mathbf{k}\sigma}^{\dagger} a_{\mathbf{k}\sigma} + \omega_{kR} b_{\mathbf{k}\sigma}^{\dagger} b_{\mathbf{k}\sigma} \right)$$

$$+ \sum_{\lambda, \sigma} \int d\mathbf{k} \left\{ \left(\phi_{\lambda}^{-}(0) v_{\mathbf{k}}^* a_{\mathbf{k}\sigma}^{\dagger} + \phi_{\lambda}^{+}(\ell) w_{\mathbf{k}}^* b_{\mathbf{k}\sigma}^{\dagger} \right) f_{\lambda\sigma} + (h.c.) \right\} .$$

Since H_{HF} is bilinear with respect to field operators, the incoming fields are linear combinations of $a_{\mathbf{k}\sigma}$, $b_{\mathbf{k}\sigma}$ and $f_{\lambda\sigma}$:

$$\alpha_{\mathbf{k}\sigma} = a_{\mathbf{k}\sigma} + \sum_{\lambda} h_{\lambda}^{\mathbf{k}} f_{\lambda\sigma} + \int d\mathbf{k}' \left(m_{\mathbf{k}'}^{\mathbf{k}} a_{\mathbf{k}'\sigma} + n_{\mathbf{k}'}^{\mathbf{k}} b_{\mathbf{k}'\sigma} \right) , \quad (\text{B}\cdot\text{4})$$

By substituting it into $[\alpha_{\mathbf{k}\sigma}, H_{\text{MF}}]/\hbar = \omega_{kL} \alpha_{\mathbf{k}\sigma}$ and comparing term by term, one has

$$\alpha_{\mathbf{k}\sigma} = a_{\mathbf{k}\sigma} + \sum_{\lambda} h_{\lambda}^{\mathbf{k}} f_{\lambda\sigma} + \int d\mathbf{k}' \left(\frac{v_{\mathbf{k}'} A_{\mathbf{k}}^{-}(0) a_{\mathbf{k}'\sigma}}{\omega_{kL} - \omega_{k'L} \pm i0} + \frac{w_{\mathbf{k}'} A_{\mathbf{k}}^{+}(\ell) b_{\mathbf{k}'\sigma}}{\omega_{kL} - \omega_{k'R} \pm i0} \right) , \quad (\text{B}\cdot\text{5})$$

$$h_{\lambda}^{\mathbf{k}} = \frac{\phi_{\lambda}^{-}(0)}{\omega_{kL} - \epsilon_{\lambda}} \{ v_{\mathbf{k}}^* + A_{\mathbf{k}}^{-}(0) \xi_{\pm}(\omega_{kL}) \} + \frac{\phi_{\lambda}^{+}(\ell)}{\omega_{kL} - \epsilon_{\lambda}} A_{\mathbf{k}}^{+}(\ell) \eta_{\pm}(\omega_{kL}) , \quad (\text{B}\cdot\text{6})$$

where $A_{\mathbf{k}}^{\rho}(x) = \sum_{\lambda} \phi_{\lambda}^{\rho}(x) h_{\lambda}^{\mathbf{k}}$ ($\rho = \pm$; $x = 0, \ell$) and

$$\xi_{\pm}(z) \equiv \int d\mathbf{k}' \frac{|v_{\mathbf{k}'}|^2}{z - \omega_{k'L} \pm i0}, \quad \eta_{\pm}(z) \equiv \int d\mathbf{k}' \frac{|w_{\mathbf{k}'}|^2}{z - \omega_{k'R} \pm i0} . \quad (\text{B}\cdot\text{7})$$

Substituting (B-6) into the definition of $A_{\mathbf{k}}^{\rho}(x)$, one obtains a linear equation for $A_{\mathbf{k}}^{-}(0)$ and $A_{\mathbf{k}}^{+}(\ell)$ and its solution is

$$A_{\mathbf{k}}^{+}(\ell) = v_{\mathbf{k}}^* \frac{g_{-+}(0, \ell : \omega_{kL})}{\Lambda_{\pm}(\omega_{kL})} , \quad (\text{B}\cdot\text{8})$$

$$v_{\mathbf{k}}^* + \xi_{\pm}(\omega_{kL}) A_{\mathbf{k}}^{-}(0) = v_{\mathbf{k}}^* \frac{1 - \eta_{\pm}(\omega_{kL}) g_{++}(\ell, \ell : \omega_{kL})}{\Lambda_{\pm}(\omega_{kL})} , \quad (\text{B}\cdot\text{9})$$

where

$$\Lambda_{\pm}(z) = 1 - \xi_{\pm}(z) g_{--}(0, 0; z) - \eta_{\pm}(z) g_{++}(\ell, \ell; z) + \xi_{\pm}(z) \eta_{\pm}(z) \{ g_{++}(\ell, \ell; z) g_{--}(0, 0; z) - g_{+-}(\ell, 0; z) g_{-+}(0, \ell; z) \} \quad (\text{B}\cdot\text{10})$$

and $g_{\rho\rho'}(x, y; z)$ is the $\rho\rho'$ -component of the Green function:

$$G(x, y; z) = \begin{pmatrix} g_{++}(x, y; z) & g_{+-}(x, y; z) \\ g_{-+}(x, y; z) & g_{--}(x, y; z) \end{pmatrix} \equiv \sum_{\lambda} \frac{\phi_{\lambda}(x) \phi_{\lambda}(y)^{\dagger}}{z - \epsilon_{\lambda}} . \quad (\text{B}\cdot\text{11})$$

As a result of the completeness of the eigenfunctions $\phi_{\lambda}(x)$, the Green function satisfies

$$\left[-i\hbar v \sigma_y \frac{\partial}{\partial x} + \Delta(x) \sigma_x \right] G(x, y; z) = \hbar z G(x, y; z) - \hbar \mathbf{1} \delta(x - y) , \quad (\text{B}\cdot\text{12})$$

$$g_{++}(0, y; z) = g_{+-}(0, y; z) = g_{-+}(\ell, y; z) = g_{--}(\ell, y; z) = 0 , \quad (\text{B}\cdot\text{13})$$

where $\mathbf{1}$ stands for the 2×2 unit matrix. Similarly, we have

$$\beta_{\mathbf{k}\sigma} = b_{\mathbf{k}\sigma} + \sum_{\lambda} \tilde{h}_{\lambda}^{\mathbf{k}} f_{\lambda\sigma} + \int d\mathbf{k}' \left(\frac{v_{\mathbf{k}'} B_{\mathbf{k}}^{-}(0) a_{\mathbf{k}'\sigma}}{\omega_{kR} - \omega_{k'L} \pm i0} + \frac{w_{\mathbf{k}'} B_{\mathbf{k}}^{+}(\ell) b_{\mathbf{k}'\sigma}}{\omega_{kR} - \omega_{k'R} \pm i0} \right), \quad (\text{B}\cdot 14)$$

$$\tilde{h}_{\lambda}^{\mathbf{k}} = \frac{\phi_{\lambda}^{-}(0)}{\omega_{kR} - \epsilon_{\lambda}} B_{\mathbf{k}}^{-}(0) \xi_{\pm}(\omega_{kR}) + \frac{\phi_{\lambda}^{+}(\ell)}{\omega_{kR} - \epsilon_{\lambda}} \{w_{\mathbf{k}}^{*} + B_{\mathbf{k}}^{+}(\ell) \eta_{\pm}(\omega_{kR})\}, \quad (\text{B}\cdot 15)$$

where $B_{\mathbf{k}}^{\rho}(x) = \sum_{\lambda} \phi_{\lambda}^{\rho}(x) \tilde{h}_{\lambda}^{\mathbf{k}}$ and

$$B_{\mathbf{k}}^{-}(0) = w_{\mathbf{k}}^{*} \frac{g_{+-}(\ell, 0 : \omega_{kR})}{\Lambda_{\pm}(\omega_{kR})}, \quad (\text{B}\cdot 16)$$

$$w_{\mathbf{k}}^{*} + \eta_{\pm}(\omega_{kR}) B_{\mathbf{k}}^{-}(\ell) = w_{\mathbf{k}}^{*} \frac{1 - \xi_{\pm}(\omega_{kR}) g_{--}(0, 0 : \omega_{kR})}{\Lambda_{\pm}(\omega_{kR})}. \quad (\text{B}\cdot 17)$$

Now we discuss the sign of small imaginary parts in the energy denominators. The sign should be chosen so that we have $e^{iH_{\text{MF}}t/\hbar} a_{\mathbf{k}\sigma} e^{-iH_{\text{MF}}t/\hbar} e^{i\omega_{kL}t} \rightarrow \alpha_{\mathbf{k}\sigma}$ and $e^{iH_{\text{MF}}t/\hbar} b_{\mathbf{k}\sigma} e^{-iH_{\text{MF}}t/\hbar} e^{i\omega_{kR}t} \rightarrow \beta_{\mathbf{k}\sigma}$, ($t \rightarrow -\infty$). From (B·5) and (B·14), original operators can be expressed in terms of the incoming fields and e.g.,

$$\begin{aligned} & e^{iH_{\text{MF}}t/\hbar} a_{\mathbf{k}\sigma} e^{-iH_{\text{MF}}t/\hbar} e^{i\omega_{kL}t} - \alpha_{\mathbf{k}\sigma} \\ &= v_{\mathbf{k}}^{*} \int d\mathbf{k}' \left\{ \frac{A_{\mathbf{k}'}^{-}(0)^{*} \alpha_{\mathbf{k}'\sigma} e^{-i(\omega_{k'L} - \omega_{kL})t}}{\omega_{k'L} - \omega_{kL} \pm i0} + \frac{B_{\mathbf{k}'}^{-}(0)^{*} \beta_{\mathbf{k}'\sigma} e^{-i(\omega_{k'R} - \omega_{kL})t}}{\omega_{k'R} - \omega_{kL} \pm i0} \right\} \end{aligned}$$

which vanishes as $t \rightarrow -\infty$ only if the lower sign is chosen since $\lim_{t \rightarrow -\infty} \frac{e^{-ixt}}{x + i0} = 0$.

Then, the electron field in the TLM chain is given by

$$\begin{aligned} \Psi_{\sigma}(x) &= \sum_{\lambda} \phi_{\lambda}(x) f_{\lambda\sigma} = \sum_{\lambda} \phi_{\lambda}(x) \int d\mathbf{k} \{h_{\lambda}^{\mathbf{k}*} \alpha_{\mathbf{k}\sigma} + \tilde{h}_{\lambda}^{\mathbf{k}*} \beta_{\mathbf{k}\sigma}\} \\ &= \int d\mathbf{k} \left\{ \frac{v_{\mathbf{k}} \alpha_{\mathbf{k}\sigma}}{\Lambda_{-}(\omega_{kL})^{*}} h(x; \omega_{kL}) + \frac{w_{\mathbf{k}} \beta_{\mathbf{k}\sigma}}{\Lambda_{-}(\omega_{kR})^{*}} \tilde{h}(x; \omega_{kR}) \right\}, \quad (\text{B}\cdot 18) \end{aligned}$$

where

$$\begin{aligned} h(x; \omega) &= G(x, 0; \omega) \begin{pmatrix} 0 \\ 1 \end{pmatrix} \{1 - g_{++}(\ell, \ell; \omega) \eta_{+}(\omega)\} \\ &\quad + G(x, \ell; \omega) \begin{pmatrix} 1 \\ 0 \end{pmatrix} g_{+-}(\ell, 0; \omega) \eta_{+}(\omega), \quad (\text{B}\cdot 19) \end{aligned}$$

$$\begin{aligned} \tilde{h}(x; \omega) &= G(x, 0; \omega) \begin{pmatrix} 0 \\ 1 \end{pmatrix} g_{-+}(0, \ell; \omega) \xi_{+}(\omega) \\ &\quad + G(x, \ell; \omega) \begin{pmatrix} 1 \\ 0 \end{pmatrix} \{1 - g_{--}(0, 0; \omega) \xi_{+}(\omega)\}. \quad (\text{B}\cdot 20) \end{aligned}$$

Appendix C

— Coulomb energy and chemical potentials —

Applying a bias voltage V to the TLM chain corresponds to the prescription $\mu_L - \mu_R = -eV$ and it alone does not determine individual values of μ_L and μ_R .

However, as will be explained below, if $\mu_L + \mu_R \neq 0$, the average number of electrons on the TLM chain increases or decreases and the whole system including ions would be electrically charged as compared with the equilibrium case. Then, such states have large electrostatic energy and are hard to be realized. Thus, one should choose $\mu_L = -\mu_R = -eV/2$.

The proof is as follows. By a similar argument to the calculation of S in (4.10), the electron number density is found to be

$$\begin{aligned} & \sum_{\sigma} \left\langle \Psi_{\sigma}^{\dagger}(x) \Psi_{\sigma}(x) \right\rangle_{\infty} \\ &= \int_{\Delta}^{\hbar\omega_c} \frac{d\epsilon}{\pi\hbar v} \frac{\epsilon}{\sqrt{\epsilon^2 - \Delta^2}} (f_L(\epsilon) + f_L(-\epsilon) + f_R(\epsilon) + f_R(-\epsilon)) , \end{aligned} \quad (\text{C}\cdot 1)$$

provided that x is not close to the chain ends. At equilibrium where $\mu_L = \mu_R = 0$, the sum of four Fermi distribution functions is equal to two and, thus, irrespective to the temperature,

$$\sum_{\sigma} \left\langle \Psi_{\sigma}^{\dagger}(x) \Psi_{\sigma}(x) \right\rangle_{\text{eq}} = \int_{\Delta}^{\hbar\omega_c} \frac{d\epsilon}{\pi\hbar v} \frac{2\epsilon}{\sqrt{\epsilon^2 - \Delta^2}} . \quad (\text{C}\cdot 2)$$

Then, as easily seen, one has

$$\begin{aligned} & \sum_{\sigma} \left\langle \Psi_{\sigma}^{\dagger}(x) \Psi_{\sigma}(x) \right\rangle_{\infty} - \sum_{\sigma} \left\langle \Psi_{\sigma}^{\dagger}(x) \Psi_{\sigma}(x) \right\rangle_{\text{eq}} \\ &= (1 - e^{-(\mu_L + \mu_R)/T}) \int_{\Delta}^{\hbar\omega_c} \frac{d\epsilon}{\pi\hbar v} \frac{\epsilon (f_L(\epsilon) f_R(-\epsilon) + f_L(-\epsilon) f_R(\epsilon))}{\sqrt{\epsilon^2 - \Delta^2}} , \end{aligned} \quad (\text{C}\cdot 3)$$

which is nonzero unless $\mu_L = -\mu_R$.

In the rest of this appendix, we show that a number of electrons per site for the open SSH chain discussed in Appendix A is approximately unity by choosing $\hbar\omega_c = \pi t_0$. Indeed, since

$$\sum_{\sigma} \langle d_{\sigma}^{\dagger}(x) d_{\sigma}(x) \rangle = \sum_{\sigma} \langle e_{\sigma}^{\dagger}(x) e_{\sigma}(x) \rangle \frac{1}{\pi v \hbar} \int_{\hbar\Delta_0}^{\hbar\omega_c} d\epsilon \frac{\epsilon}{\sqrt{\epsilon^2 - \Delta_0^2}} \approx \frac{\omega_c}{\pi v}$$

and $v = 2at_0/\hbar$, a number of electrons per site is

$$\sum_{\sigma} \langle C_{2n,\sigma}^{\dagger} C_{2n,\sigma} \rangle = \sum_{\sigma} \langle C_{2n-1,\sigma}^{\dagger} C_{2n-1,\sigma} \rangle \approx \frac{\hbar\omega_c}{\pi t_0} = 1 .$$

Appendix D

— Green function for spatially uniform phase —

In this appendix, we explicitly write down the Green function defined by (3.11) in the spatially uniform case:

$$g_{++}(x, y; \omega) = \begin{cases} -\frac{\omega(\hbar\kappa v \cos \kappa(\ell - y) + \bar{\Delta} \sin \kappa(\ell - y)) \sin \kappa x}{\kappa v^2 D(\omega)} & (x < y) \\ -\frac{\omega(\hbar\kappa v \cos \kappa(\ell - x) + \bar{\Delta} \sin \kappa(\ell - x)) \sin \kappa y}{\kappa v^2 D(\omega)} & (x > y) \end{cases} \quad (\text{D}\cdot 1)$$

$$g_{--}(x, y; \omega) = \begin{cases} -\frac{\omega(\hbar\kappa v \cos \kappa x + \bar{\Delta} \sin \kappa x) \sin \kappa(\ell - y)}{\kappa v^2 D(\omega)} & (x < y) \\ -\frac{\omega(\hbar\kappa v \cos \kappa y + \bar{\Delta} \sin \kappa y) \sin \kappa(\ell - x)}{\kappa v^2 D(\omega)} & (x > y) \end{cases} \quad (\text{D}\cdot 2)$$

$$\begin{aligned} g_{+-}(x, y; \omega) &= g_{-+}(y, x; \omega) \\ &= \begin{cases} -\frac{\hbar\omega^2 \sin \kappa(\ell - y) \sin \kappa x}{\kappa v^2 D(\omega)} & (x < y) \\ -\frac{(\hbar\kappa v \cos \kappa y + \bar{\Delta} \sin \kappa y)(\hbar\kappa v \cos \kappa(\ell - x) + \bar{\Delta} \sin \kappa(\ell - x))}{\hbar\kappa v^2 D(\omega)} & (x > y) \end{cases} \end{aligned} \quad (\text{D}\cdot 3)$$

where $\kappa = \sqrt{(\hbar\omega)^2 - \bar{\Delta}^2}/(\hbar v)$ and $D(\omega) = \hbar\kappa v \cos \kappa\ell + \bar{\Delta} \sin \kappa\ell$.

Appendix E

— Stability of fixed points —

In this appendix, we show that nontrivial solutions of (4.9) are more stable at constant current than those at constant bias voltage. Then, we prove that, at constant current, the zero-temperature ordered phase with $\bar{\Delta}$ given by (5.13) is stable.

Firstly, we note that the stability indices χ_V at constant bias voltage and χ_I at constant current differ by

$$\chi_I(\bar{\Delta}) - \chi_V(\bar{\Delta}) = -\lambda \bar{\Delta} \left(\frac{\partial S}{\partial V} \right)_{\bar{\Delta}} \left(\frac{\partial \bar{J}}{\partial \bar{\Delta}} \right)_V \bigg/ \left(\frac{\partial \bar{J}}{\partial V} \right)_{\bar{\Delta}}. \quad (\text{E}\cdot 1)$$

As easily seen, we have

$$\frac{eT}{\sinh\left(\frac{eV}{2T}\right)} \left(\frac{\partial S}{\partial V} \right)_{\bar{\Delta}} = \int_{\bar{\Delta}}^{\hbar\omega_c} \frac{d\epsilon}{\sqrt{\epsilon^2 - \bar{\Delta}^2}} \frac{e^2 \sinh\left(\frac{\epsilon}{T}\right)}{\left\{ \cosh\left(\frac{eV}{2T}\right) + \cosh\left(\frac{\epsilon}{T}\right) \right\}^2} > 0$$

$$\begin{aligned} \left(\frac{\partial \bar{J}}{\partial V}\right)_{\bar{\Delta}} &= \frac{G_0}{T} \int_{\bar{\Delta}}^{\hbar\omega_c} d\epsilon \frac{\sqrt{\epsilon^2 - \bar{\Delta}^2}}{\epsilon} \frac{1 + \cosh\left(\frac{eV}{2T}\right) \cosh\left(\frac{\epsilon}{T}\right)}{\left\{\cosh\left(\frac{eV}{2T}\right) + \cosh\left(\frac{\epsilon}{T}\right)\right\}^2} > 0 \\ \frac{e\bar{\Delta}}{\sinh\left(\frac{eV}{2T}\right)} \left(\frac{\partial \bar{J}}{\partial \bar{\Delta}}\right)_V &= - \int_{\bar{\Delta}}^{\hbar\omega_c} d\epsilon \frac{2G_0\bar{\Delta}^2}{\epsilon\sqrt{\epsilon^2 - \bar{\Delta}^2} \left\{\cosh\left(\frac{eV}{2T}\right) + \cosh\left(\frac{\epsilon}{T}\right)\right\}} < 0. \end{aligned}$$

Thus, $\chi_I(\bar{\Delta}) > \chi_V(\bar{\Delta})$ which implies that the phase is more stable at constant current than at constant bias voltage.

Now, let us study the stability of the ordered phase given by (5.13) at constant current. It is easy to show

$$\bar{\Delta} \left(\frac{\partial S}{\partial V}\right)_{\bar{\Delta}} \left(\frac{\partial \bar{J}}{\partial \bar{\Delta}}\right)_V / \left(\frac{\partial \bar{J}}{\partial V}\right)_{\bar{\Delta}} = \frac{2r}{r^2 - 1} \left(\int_1^r dx \frac{\sqrt{x^2 - 1}}{x} - \sqrt{r^2 - 1} \right), \quad (\text{E.2})$$

where $r \equiv |eV/2\bar{\Delta}| > 1$. Thus, we obtain the desired result:

$$\begin{aligned} \chi_I &= 2\lambda \left(\frac{\hbar\omega_c}{\sqrt{(\hbar\omega_c)^2 - |\bar{\Delta}|^2}} - 1 \right) + \frac{2\lambda r}{r^2 - 1} \left\{ r - \frac{1}{r} - \int_1^r dx \frac{\sqrt{x^2 - 1}}{x} \right\} \\ &= 2\lambda \left(\frac{\hbar\omega_c}{\sqrt{(\hbar\omega_c)^2 - |\bar{\Delta}|^2}} - 1 \right) + \frac{2\lambda r}{r^2 - 1} \int_1^r dx \left\{ 1 + \frac{1}{x^2} - \frac{\sqrt{x^2 - 1}}{x} \right\} \\ &= 2\lambda \left(\frac{\hbar\omega_c}{\sqrt{(\hbar\omega_c)^2 - |\bar{\Delta}|^2}} - 1 \right) + \frac{2\lambda r}{r^2 - 1} \int_1^r dx \frac{1 + 3x^2}{x^2(x^2 + 1 + x\sqrt{x^2 - 1})} > 0. \end{aligned}$$

Appendix F

— Ginzburg-Landau expansion coefficients —

In this appendix, we list up the coefficients K_2 and K_4 introduced in (5.23) when $\hbar\omega_c \gg T$. By letting $\hbar\omega_c/T \rightarrow \infty$ in $S(\bar{\Delta}, V, T) - S(0, V, T)$ and Taylor-expanding the result with respect to $\bar{\Delta}/T$, we obtain the desired expansion:

$$0 = \frac{1}{2\lambda} + \frac{1}{2} S(0, V, T) + \frac{S(\bar{\Delta}, V, T) - S(0, V, T)}{2} = \frac{\chi_N}{2\lambda} - \frac{K_2 \bar{\Delta}^2}{2T^2} + \frac{K_4 \bar{\Delta}^4}{8T^4}, \quad (\text{F.1})$$

where K_2 and K_4 are functions of $eV/(2T)$ defined by

$$\begin{aligned} K_2 &= \int_0^\infty \frac{dt}{t} \frac{d}{dt} \left(\frac{\sinh t}{t(\cosh(eV/(2T)) + \cosh t)} \right), \\ K_4 &= - \int_0^\infty \frac{dt}{t} \frac{d}{dt} \left\{ \frac{1}{t} \frac{d}{dt} \left(\frac{\sinh t}{t(\cosh(eV/(2T)) + \cosh t)} \right) \right\}. \end{aligned} \quad (\text{F.2})$$

References

- 1) O. Bratteli and D.W. Robinson: *Operator Algebras and Quantum Statistical Mechanics* vol.1, vol.2, (Springer, Berlin-Heidelberg-New York, 2002).

- 2) R. Haag: *Local Quantum Physics* (Springer, Berlin-Heidelberg-New York, 1996).
- 3) S. Attal, A. Joye, and C.-A. Pillet (Eds.): *Open Quantum Systems I, II, III* (Lecture Notes in Mathematics, 1880, 1881, 1882) (Springer, Berlin-Heidelberg-New York, 2006).
- 4) W. Pusz and S. L. Woronowicz: *Commun. Math. Phys.* **58**, 273 (1978).
- 5) I.Ojima, H.Hasegawa and M. Ichiyanagi: *J. Stat. Phys.* **50**, 633 (1988); I.Ojima: *J. Stat. Phys.* **56**, 203 (1989); I. Ojima, in *Quantum Aspects of Optical Communications*, eds. C. Bendjaballah, O. Hirota, and S. Reynaud, p.164 (LNP **378**, Springer, 1991).
- 6) T.G. Ho and H. Araki: *Proc. Steklov Math. Institute* **228**, 191 (2000); W. Aschbacher and C.-A. Pillet: *J. Stat. Phys.* **112**, 1153 (2003).
- 7) D. Ruelle: *J. Stat. Phys.* **98**, 57 (2000); *Comm. Math. Phys.* **224**, 3 (2001); “Topics in quantum statistical mechanics and operator algebras” math-ph/0107009 (2001).
- 8) V. Jakšić and C.-A. Pillet: *Commun. Math. Phys.* **217**, 285 (2001); *Commun. Math. Phys.* **226**, 131 (2002); *J. Stat. Phys.* **108**, 269 (2002).
- 9) W. Aschbacher, V. Jakšić, Y. Pautrat, and C.-A. Pillet: “Topics in nonequilibrium quantum statistical mechanics”, in vol. III of Ref.3).
- 10) J. Fröhlich, M. Merkli, S. Schwarz, and D. Ueltschi: *A garden of quanta*, eds. J. Arafune, A. Arai, M. Kobayashi, K. Nakamura, p.345 (World Scientific, River Edge, 2003).
- 11) S. Tasaki and T. Matsui: in *Fundamental Aspects of Quantum Physics* eds. L.Accardi and S.Tasaki, p.100 (World Scientific, Singapore, 2003).
- 12) S. Tasaki and J. Takahashi: *Prog. Theor. Phys. Suppl.* **165** 57 (2006).
- 13) S. Tasaki: *J. Phys.:Conf. Ser.* **31**, 35 (2006); S. Tasaki and T. Matsui: RIMS Kohkyuroku, No.1507, p.118 (2006) math-ph/0605051.
- 14) V. Jakšić, Y. Ogata, and C.-A. Pillet: *Comm. Math. Phys.*, **265** 721 (2006); *ibid.* **268** 369 (2006); *J Stat. Phys.*, **123** 547 (2006); *Ann. Henri Poincaré*, **8** 1013 (2007).
- 15) W. Salem and J. Fröhlich, *J. Stat. Phys.*, **126** 1045 (2007); W.K. Abou Salem, *Ann. Henri Poincaré* **8** 569 (2007).
- 16) W. Aschbacher, V. Jakšić, Y. Pautrat, and C.-A. Pillet: *J. Math. Phys.* **48** 032101 (2007); G. Nenciu, *J. Math. Phys.* **48** 033302 (2007); J. Fröhlich, M. Merkli, and D. Ueltschi: *Ann. Henri Poincaré* **4**, 897 (2003); S. Tasaki: *Chaos, Solitons and Fractals* **12**, 2657 (2001).
- 17) J. Takahashi and S. Tasaki: *Physica E* **34** 651 (2006); *J. Phys. Soc. Jpn Supp.* **74** 261 (2005).
- 18) J. Dereziński and R. Fruboos: “Fermi Golden Rule and open quantum systems”, in vol. III of Ref.3); V. Jakšić and C.-A. Pillet: *Contemporary Mathematics*, **447** 153 (2007); M. Merkli, I.M. Sigal, and G.P. Berman: *Ann. Phys.* **323** 373 (2008); M. Merkli, M. Mueck, and I.M. Sigal: *Ann. Henri Poincaré* **8** 1539 (2007); H.D. Cornean, H. Neidhardt, and V.A. Zagrebnoy: “ The effect of time-dependent coupling on nonequilibrium steady”, (2007) arXiv:0708.3931.
- 19) Ya. M. Blanter and M. Büttiker: *Phys. Rep.* **336** 1 (2000).
- 20) H. Katsura: *J. Phys. Soc. Jpn.*, **76** 054710 (2007).
- 21) J. Takahashi and S. Tasaki: *J. Phys. Soc. Jpn* **75** 094712 (2006).
- 22) H. Takayama, Y.-R. Lin-Liu, and K. Maki: *Phys. Rev. B* **21**, 2388 (1980).
- 23) W. P. Su, J. R. Schrieffer, and A. J. Heeger: *Phys. Rev. Lett.* **42**, 1698 (1979); *Phys. Rev. B* **22**, 2099 (1980).
- 24) K. Inagaki, I. Terasaki, H. Mori, and T. Mori: *J. Phys. Soc. Jpn.* **73**, 3364 (2004).
- 25) F. Sawano, I. Terasaki, H. Mori, T. Mori, M. Watanabe, N. Ikeda, Y. Nogami, and Y. Noda: *Nature* **437** 522 (2005).
- 26) M. Watanabe, K. Yamamoto, T. Ito, Y. Nakashima, M. Tanabe, N. Hanasaki, N. Ikeda, Y. Nogami, H. Ohsumi, H. Toyokawa, Y. Noda, I. Terasaki, F. Sawano, T. Suko, H. Mori, and T. Mori: *J. Phys. Soc. Jpn.* **77**, 065004 (2008).
- 27) F. Sawano, T. Suko, T. S. Inada, S. Tasaki, I. Terasaki, H. Mori, T. Mori, Y. Nogami, N. Ikeda, M. Watanabe, and Y. Noda: *J. Phys. Soc. Jpn.* **78** 024714 (2009).
- 28) G. Benenti, G. Casati, T. Prosen and D. Rossini: *Europhys. Lett.* **85** 37001 (2009); T. Prosen, arXiv0704.2252 (2007).
- 29) R. Egger, A. Grabert, A. Koutouza, H. Saleur, and F. Siano: *Phys. Rev. Lett.* **84**, 3682 (2000); A. Koutouza, F. Siano, and H. Saleur: *J. Phys. A: Math. Gen.* **34** 5497 (2001).
- 30) T. Oka, R. Arita, and H. Aoki, *Phys. Rev. Lett.* **91** 066406 (2003).
- 31) G. Benenti, G. Casati, T. Prosen, D. Rossini, and M. Žnidarič: arXiv0901.2032 (2009).
- 32) C. S. Owen and D. J. Scalapino, *Phys. Rev. Lett.* **28**, 1559 (1972).

- 33) J.-J. Chang and D. J. Scalapino, Phys. Rev. B **10**, 4047 (1974).
- 34) G. Grüner, *Density Waves in Solids*, (Addison-Wesley Longmans, Reading, 1994).
- 35) Y. Takahide, T. Konoike, K. Enomoto, M. Nishimura, T. Terashima, S. Uji, and H. M. Yamamoto: Phys. Rev. Lett. **96** 136602 (2006).